

# Supporting Information

## Advanced Trifunctional Electrodes for 1.5 V-based Self-Powered Aqueous Electrochemical Energy Device

Ran Xiao,<sup>a</sup> Peng Huang,<sup>a</sup> Tuzhi Xiong,<sup>a</sup> Jingjing Wei,<sup>a</sup> Feng Wang,<sup>b</sup> Jianqiu Deng,<sup>b</sup> Zhongmin Wang,<sup>\*,c</sup> and M.-Sadeeq (Jie Tang) Balogun<sup>\*,a,b</sup>

### Synthesis of NiFe-LDH/NF

5 mmol  $\text{Fe}(\text{NO}_3)_2 \cdot 9\text{H}_2\text{O}$ , 15 mmol  $\text{Ni}(\text{NO}_3)_2 \cdot 6\text{H}_2\text{O}$  and 37.5 mmol Triethanolamine were mixed and stirred for 1 h in 200 mL deionized (DI) water, next stirred for 30 min with a piece of NF (3 × 4 cm<sup>2</sup>). The 60 mL mixture and NF were transferred to a 100 mL Teflon-lined stainless-steel autoclave and warmed up to 150 °C and maintained for 48 h. The NiFe-LDH/NF was washed with DI water and ethanol several times and dried in a vacuum at 60 °C. Detailed characterization can be found in Figure S18.

### DFT Calculations

All the calculations were performed with the ABINIT software package. Total energy calculations were performed to study the properties of  $\text{Ni}_3\text{N}$  structure using the periodic

density functional theory (DFT) and density functional perturbation theory (DFPT) which were implemented in ABINIT code. ABINIT stands for “Open-Source Package for Research in Electronic Structure, Simulation, and Optimization”.<sup>1</sup> *Exchange-correlation energy* was treated with the generalized gradient approximation (GGA) using the Perdew, Burke, and Enzerhof (PBE) parameterization.<sup>2</sup> The electron-ion interaction was modeled using the pseudo-potential generated by Van Setten et al., which gives very transferable norm conservation pseudo-potentials.<sup>3</sup> Integrations in the reciprocal lattice were made using the k-points generation method of Monkhorst and Pack.<sup>4</sup> Population analysis has been performed on the optimized structures in the ground state. Charge transfer analysis and electron density differences were performed with Multiwfn 3.2.1.<sup>5</sup> Models of Ni<sub>3</sub>N were used to simulate the V-Ni<sub>3</sub>N, Fe-Ni<sub>3</sub>N, and V-Fe-Ni<sub>3</sub>N samples. In the Supporting Information, we have outlined the models and how they have been built.

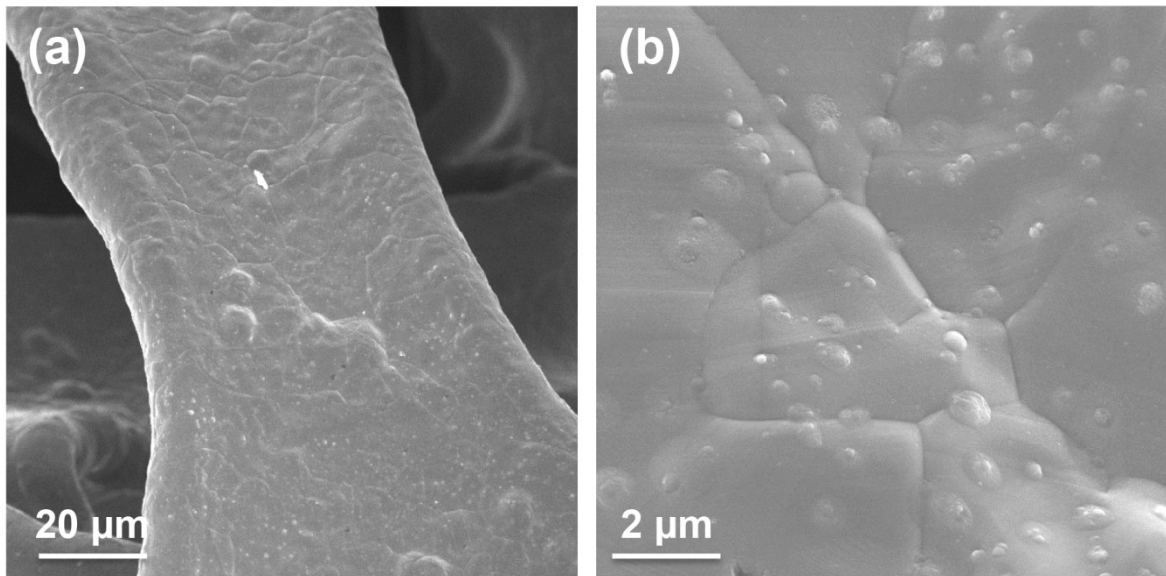


**Figure S1.** (a, b) SEM images of NF.

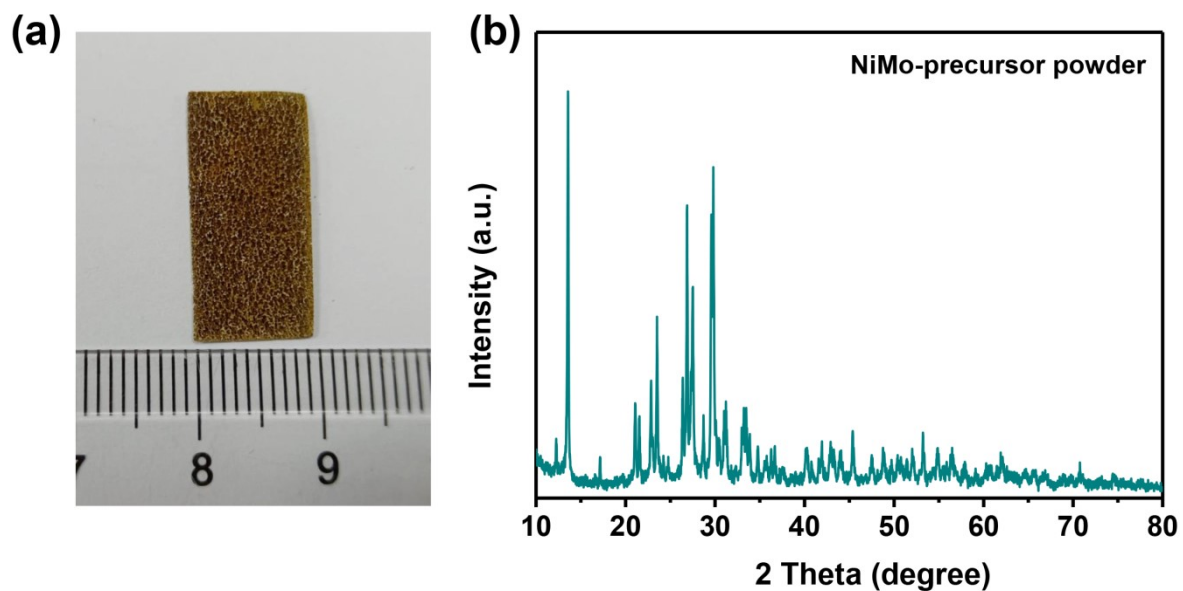


**Figure S2.** (a) Digital image of NiMo precursor. (b) XRD pattern of NiMo precursor.

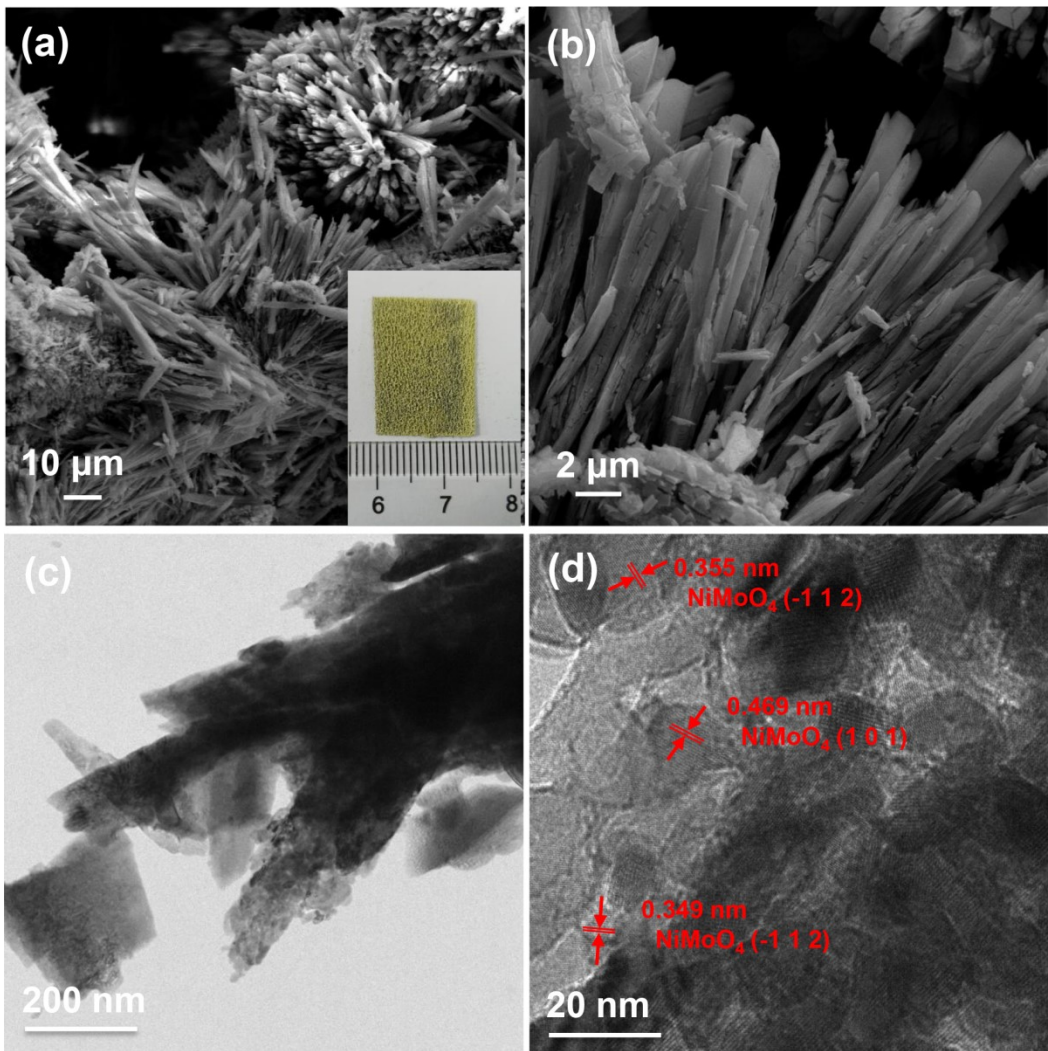


**Figure S3.** (a, b) SEM and (c, d) TEM images of pristine NMO.

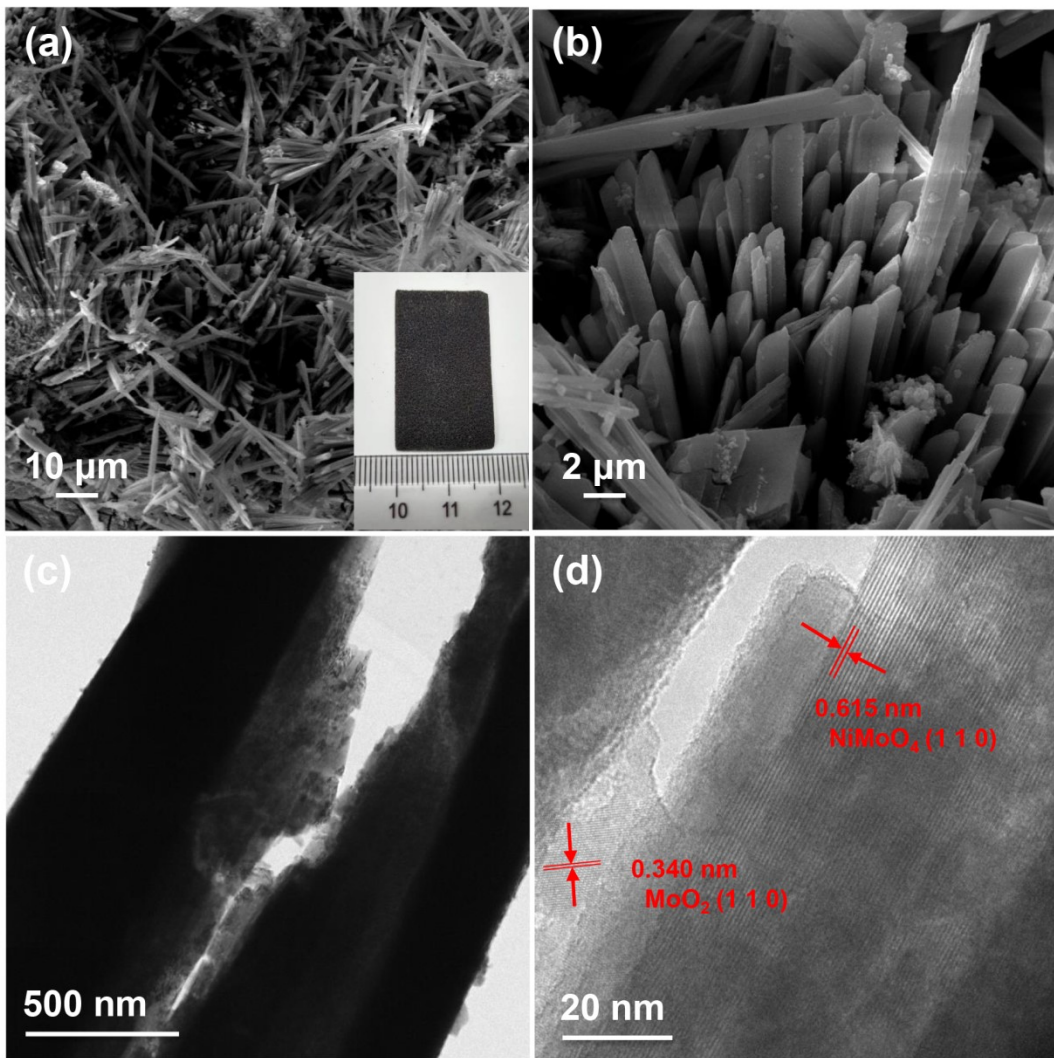


**Figure S4.** (a, b) SEM and (c, d) TEM images of NMO-MO.

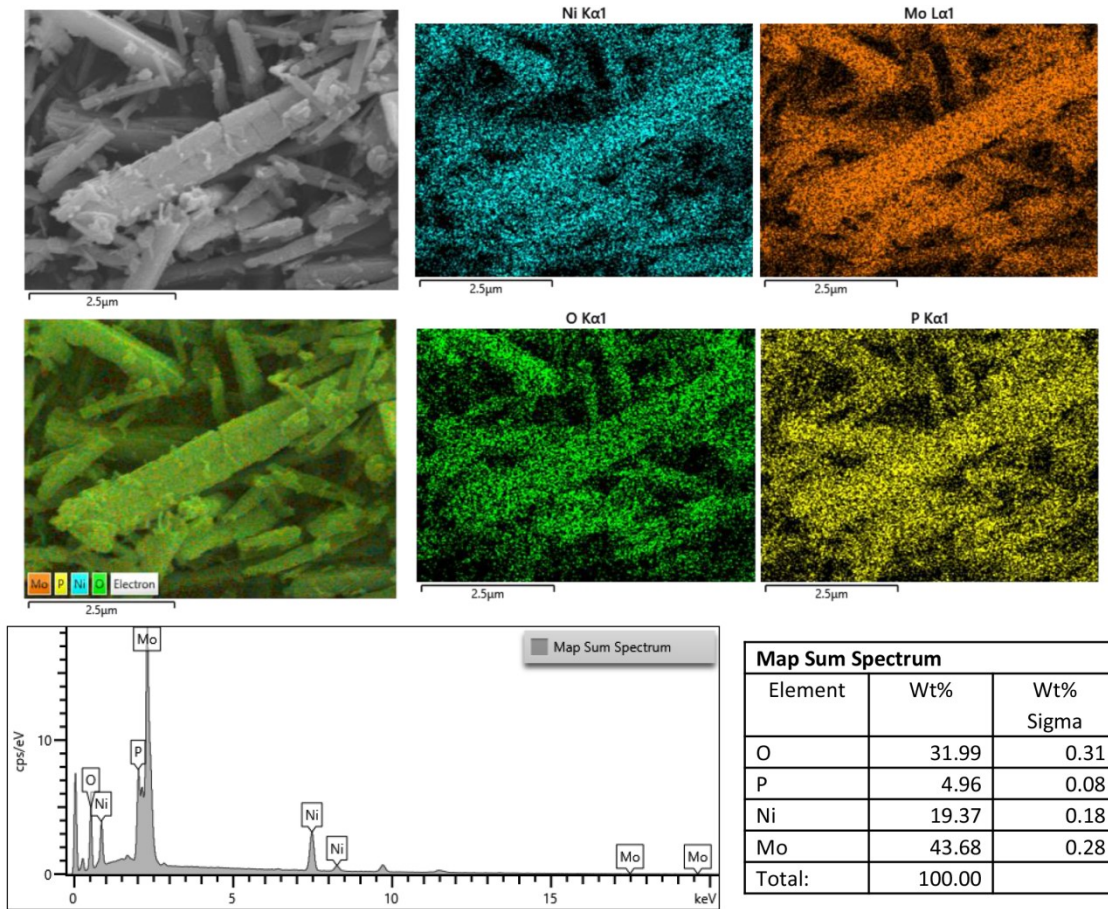


**Figure S5.** SEM elemental mapping results of NMO-MO-P sample.

**Table S1.** ICP data for atomic percentage (%) of the samples.

Element Sample \	Ni	Mo	O	P
NMO	23.0	42.6	34.4	/
NMO-MO	22.3	39.1	38.6	/
NMO-MO-P	19.8	43.1	30.2	6.9

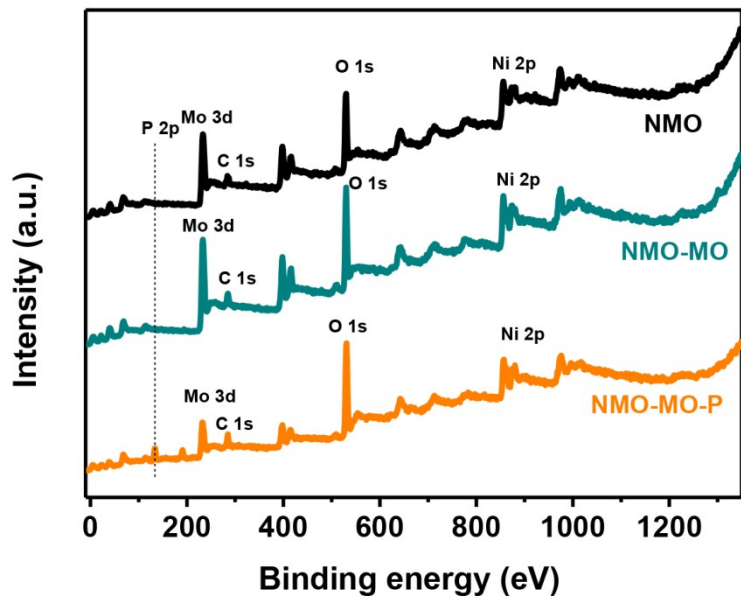


**Figure S6.** (a) Survey XPS spectra of NMO, NMO-MO and NMO-MO-P samples.

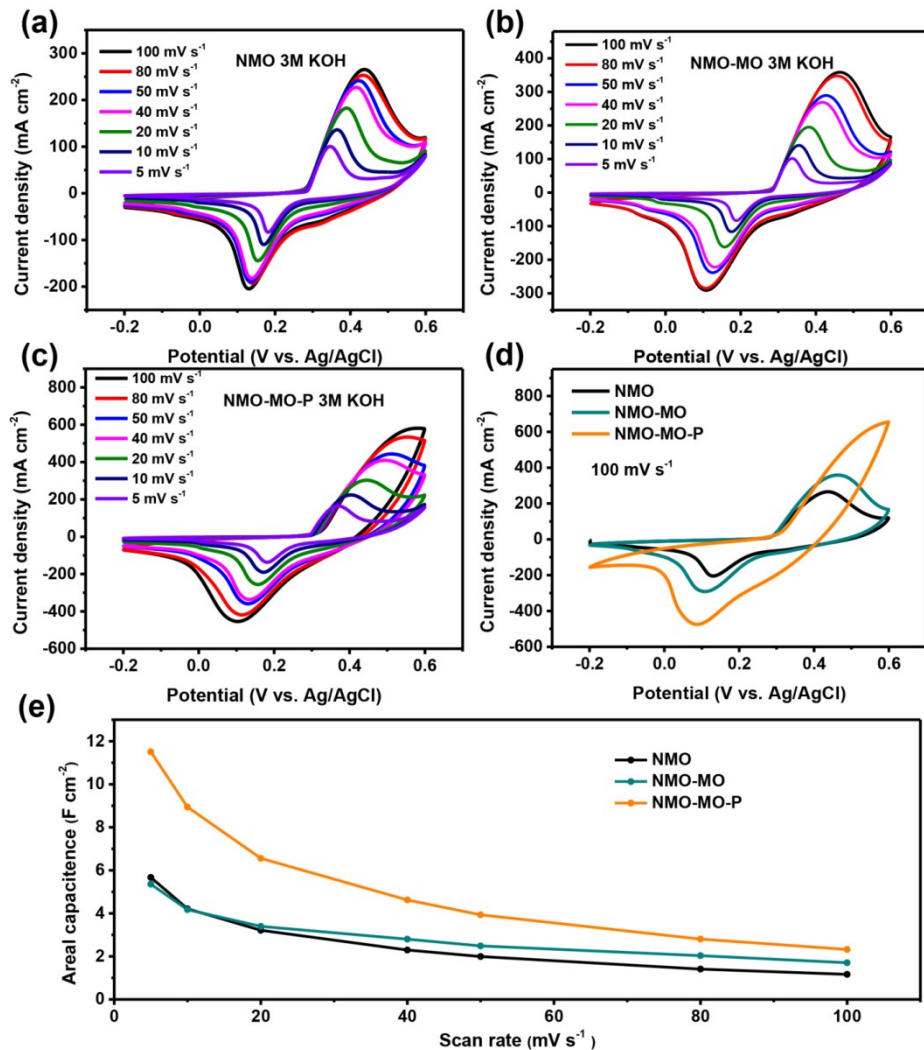


**Figure S7.** (a-c) CV curves of NMO, NMO-MO and NMO-MO-P electrodes. (d) CV curves of the different electrodes at the scan rate of 100  $\text{mV s}^{-1}$ . (e) Areal capacitance of the different electrodes as a function of scan rate.

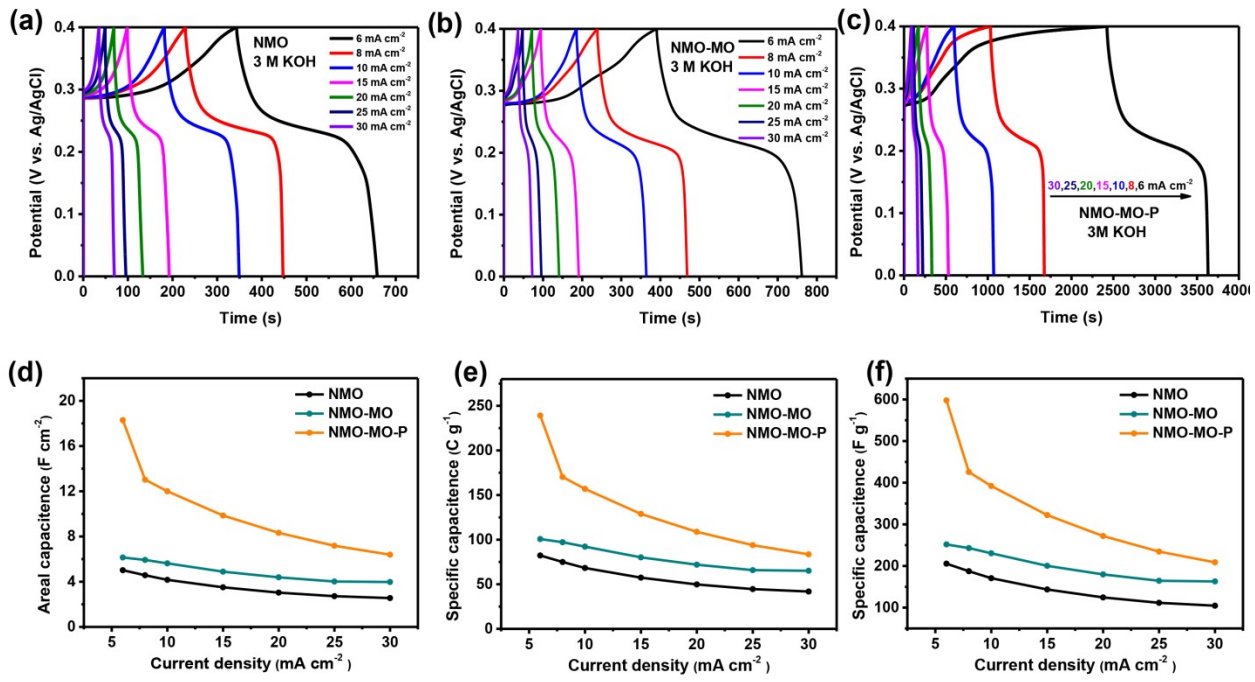


**Figure S8.** (a-c) GCD curves of NMO, NMO-MO and NMO-MO-P electrodes. (d) Areal capacitance and (e, f) specific capacitance of the different electrodes as a function of current density.

**Table S2.** Areal capacitance comparison of the positive electrode performance of our as-prepared NMO-MO-P NRs to other NMO-based electrodes.

Electrodes	Electrolyte	Areal Capacitance
NMO-MO-P (Our work)	3 M KOH	7.32 C cm <sup>-2</sup> , 18.29 F cm <sup>-2</sup> (6 mA cm <sup>-2</sup> )
	2 M KOH	4.10 C cm <sup>-2</sup> , 10.24 F cm <sup>-2</sup> (6 mA cm <sup>-2</sup> )
	1 M KOH	2.58 C cm <sup>-2</sup> , 6.46 F cm <sup>-2</sup> (6 mA cm <sup>-2</sup> )
Co-Mg compound@NiMoO <sub>4</sub> <sup>6</sup>	6 M KOH	6.50 F cm <sup>-2</sup> (5 mA cm <sup>-2</sup> )
NiCo <sub>2</sub> O <sub>4</sub> @NiMoO <sub>4</sub> /PANI <sup>7</sup>	PVA/H <sub>3</sub> PO <sub>4</sub>	2.38 F cm <sup>-2</sup> (1 mA cm <sup>-2</sup> )
NiMoO <sub>4</sub> /Ni film/Cu <sup>8</sup>	2 M NaOH	12.03 F cm <sup>-2</sup> (4 mA cm <sup>-2</sup> )
NiMoO <sub>4</sub> NSS-CNTs-CuO NWAs/Cu <sup>9</sup>	6 M KOH	23.40 F cm <sup>-2</sup> (2 mA cm <sup>-2</sup> )
NiMoO <sub>4</sub> @CoMoO <sub>4</sub> <sup>10</sup>	6 M KOH	5.4 F cm <sup>-2</sup> (2 mA cm <sup>-2</sup> )
PPy/NiMoO <sub>4</sub> /CC <sup>11</sup>	2 M KOH	3.40 F cm <sup>-2</sup> (5 mA cm <sup>-2</sup> )
NiMoO <sub>4</sub> /NiO <sup>12</sup>	3 M KOH	10.3 F cm <sup>-2</sup> (11 mA cm <sup>-2</sup> )
NiCo <sub>2</sub> O <sub>4</sub> -UNSA@NiMoO <sub>4</sub> <sup>13</sup>	3 M KOH	7.29 F cm <sup>-2</sup> (2 mA cm <sup>-2</sup> )
P-CoCH@NiMoO <sub>4</sub> <sup>14</sup>	1 M KOH	5.08 F cm <sup>-2</sup> (2 mA cm <sup>-2</sup> )
Zn–Mo–Ni–O–S HMF <sup>15</sup>	6 M KOH	6.27 F cm <sup>-2</sup> (1 mA cm <sup>-2</sup> )
NiMoP@CoCH/CC <sup>16</sup>	1 M KOH	4.0 F cm <sup>-2</sup> (1 mA cm <sup>-2</sup> )

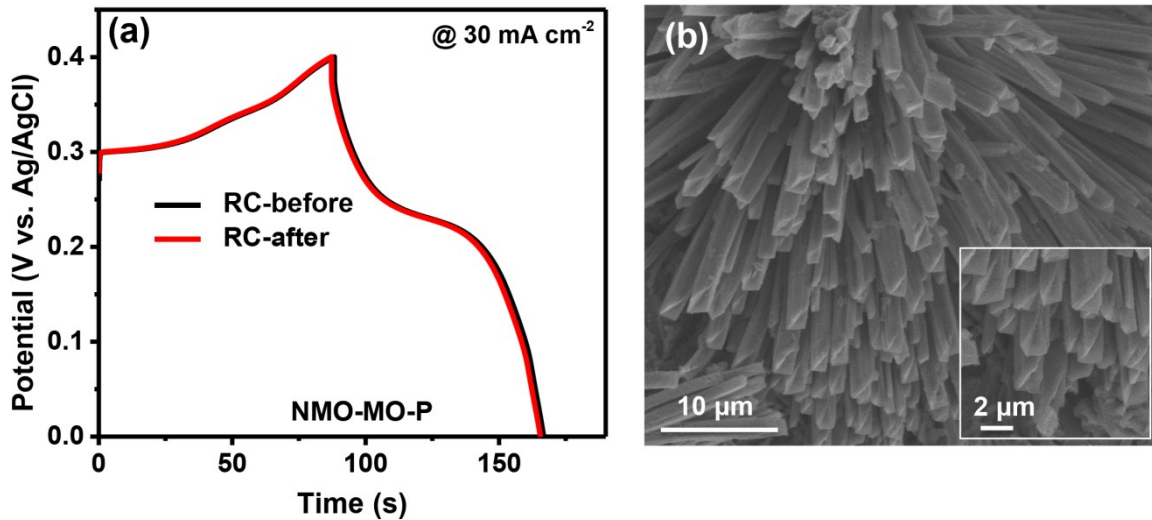


**Figure S9.** (a) GCD curves of NMO-MO-P electrode before and after the rate cycle. (b) SEM images of NMO-MO-P electrode after stability test.

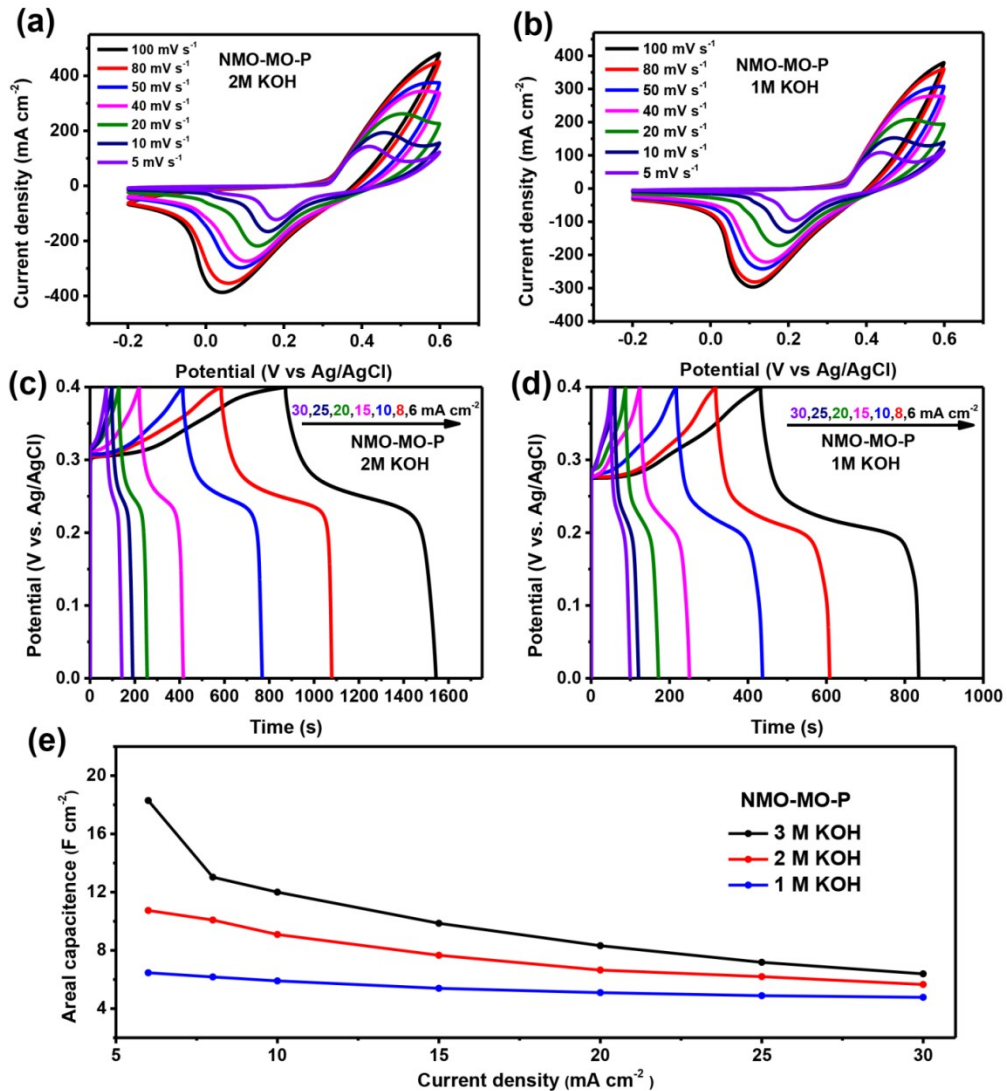


**Figure S10.** (a, b) CV curves and (c, d) GCD curves of NMO-MO-P electrode in 2.0 M and 1.0 M KOH electrolyte. (e) Areal capacitance of the NMO-MO-P electrodes as a function of current density in different electrolyte concentration.

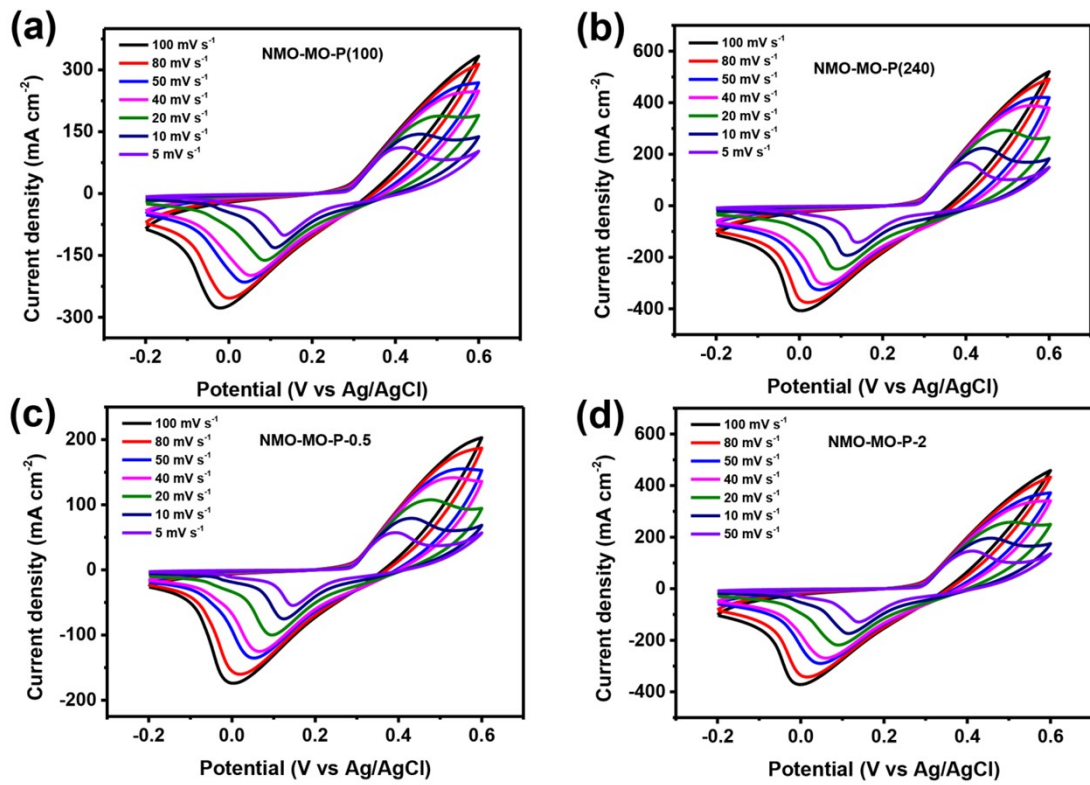


**Figure S11.** (a-d) CV curves of NMO-MO-P(100), NMO-MO-P(240), NMO-MO-P-0.5 and NMO-MO-P-2 in 3 M KOH.

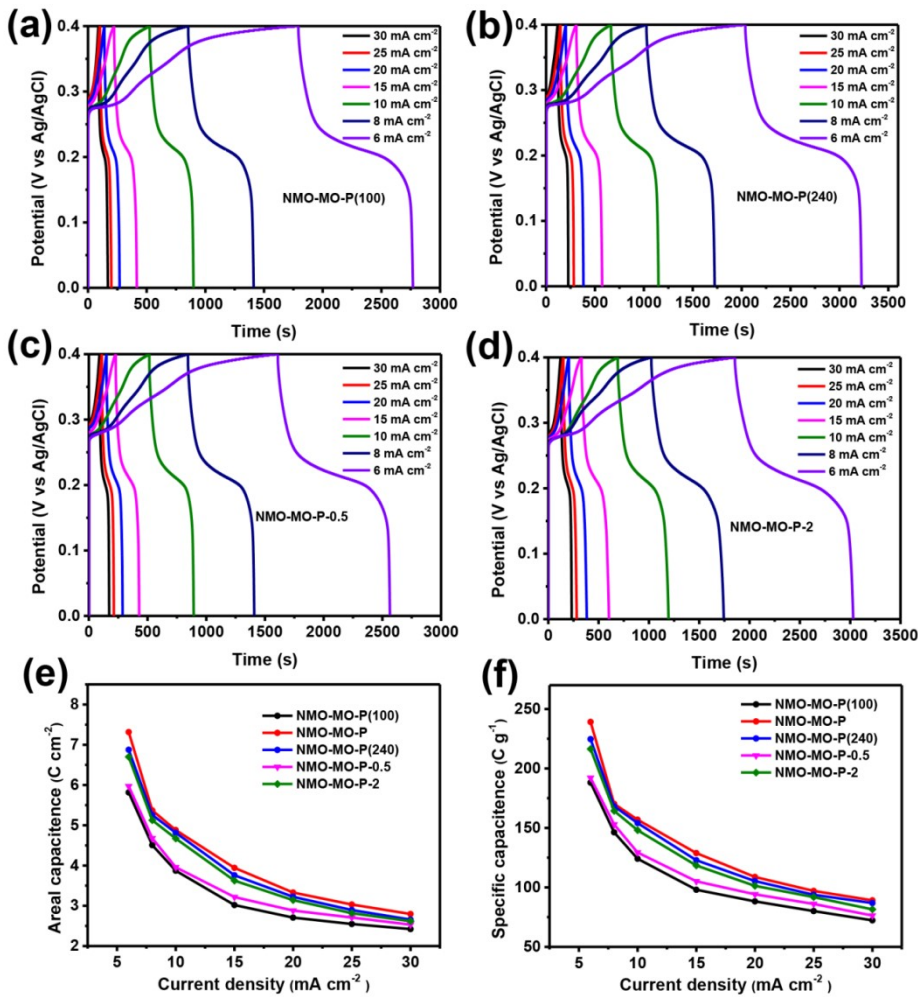


**Figure S12.** (a-d) GCD curves of NMO-MO-P(100), NMO-MO-P(240), NMO-MO-P-0.5 and NMO-MO-P-2 in 3 M KOH. (e) Areal capacitance and (f) specific capacitance as a function of current density of MO-MO-P(100), NMO-MO-P(240), NMO-MO-P-0.5 and NMO-MO-P-2 in 3 M KOH.

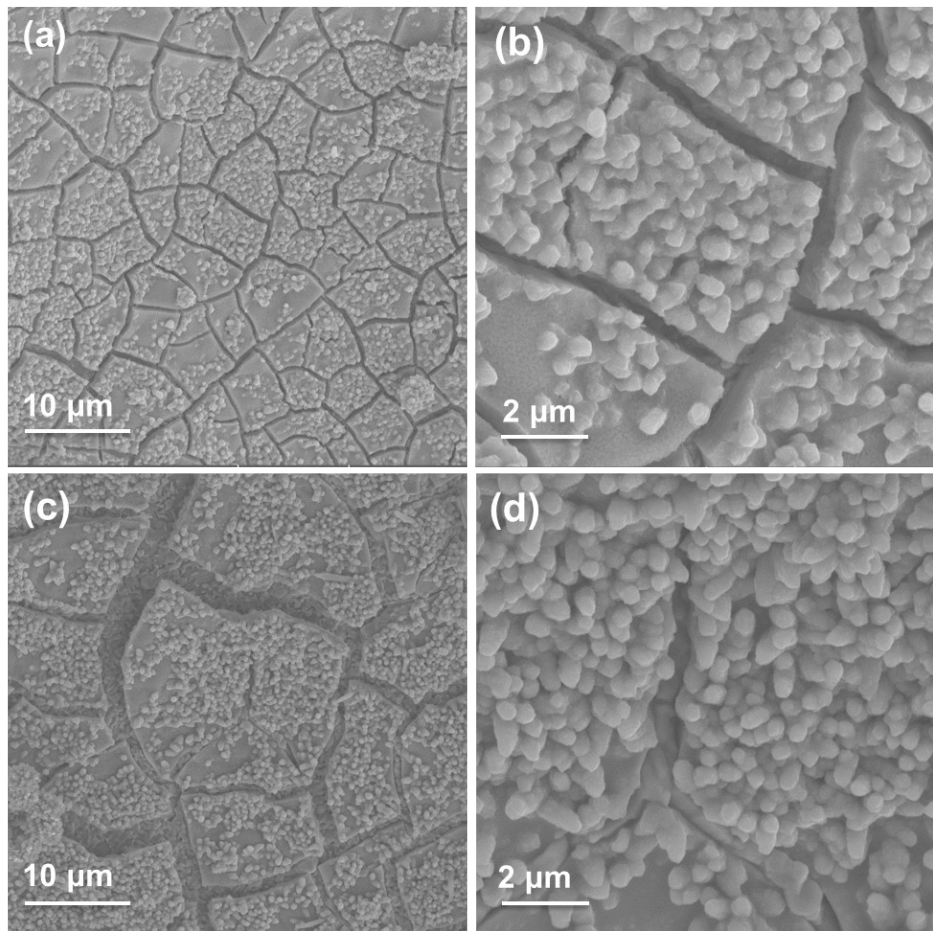


**Figure S13.** SEM images of (a, b) Mo-Ar and (c, d) Mo-Ar-P.

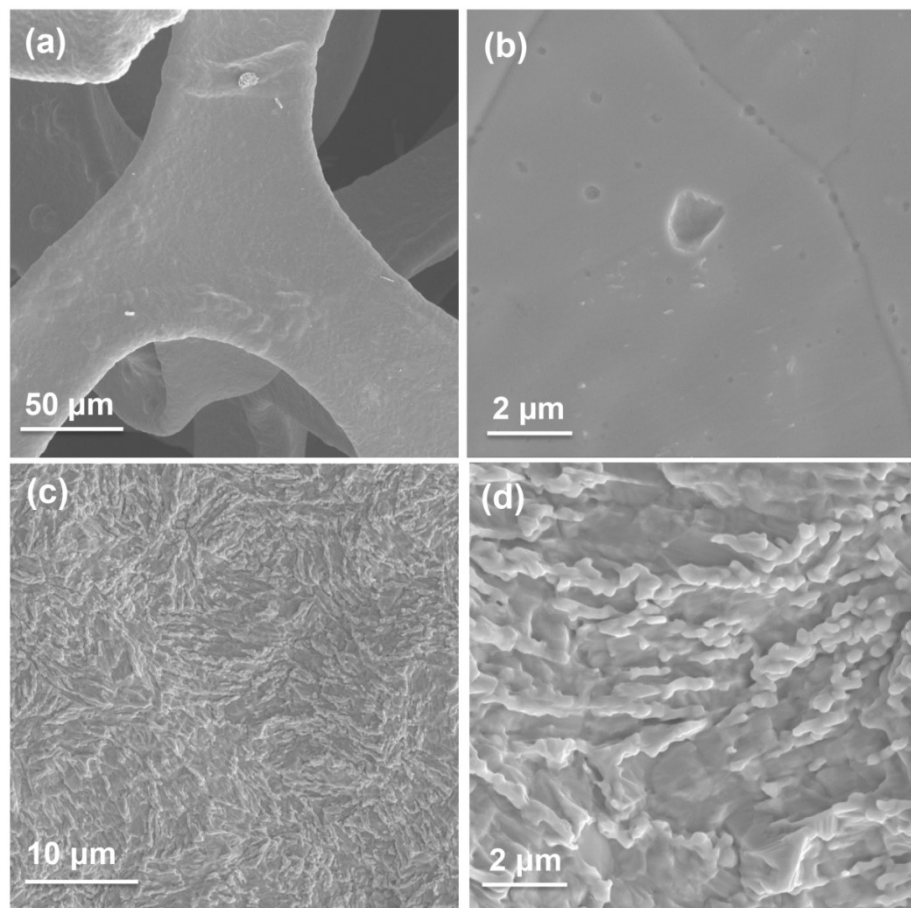


**Figure S14.** SEM images of (a, b) Ni-Ar and (c, d) Ni-Ar-P.

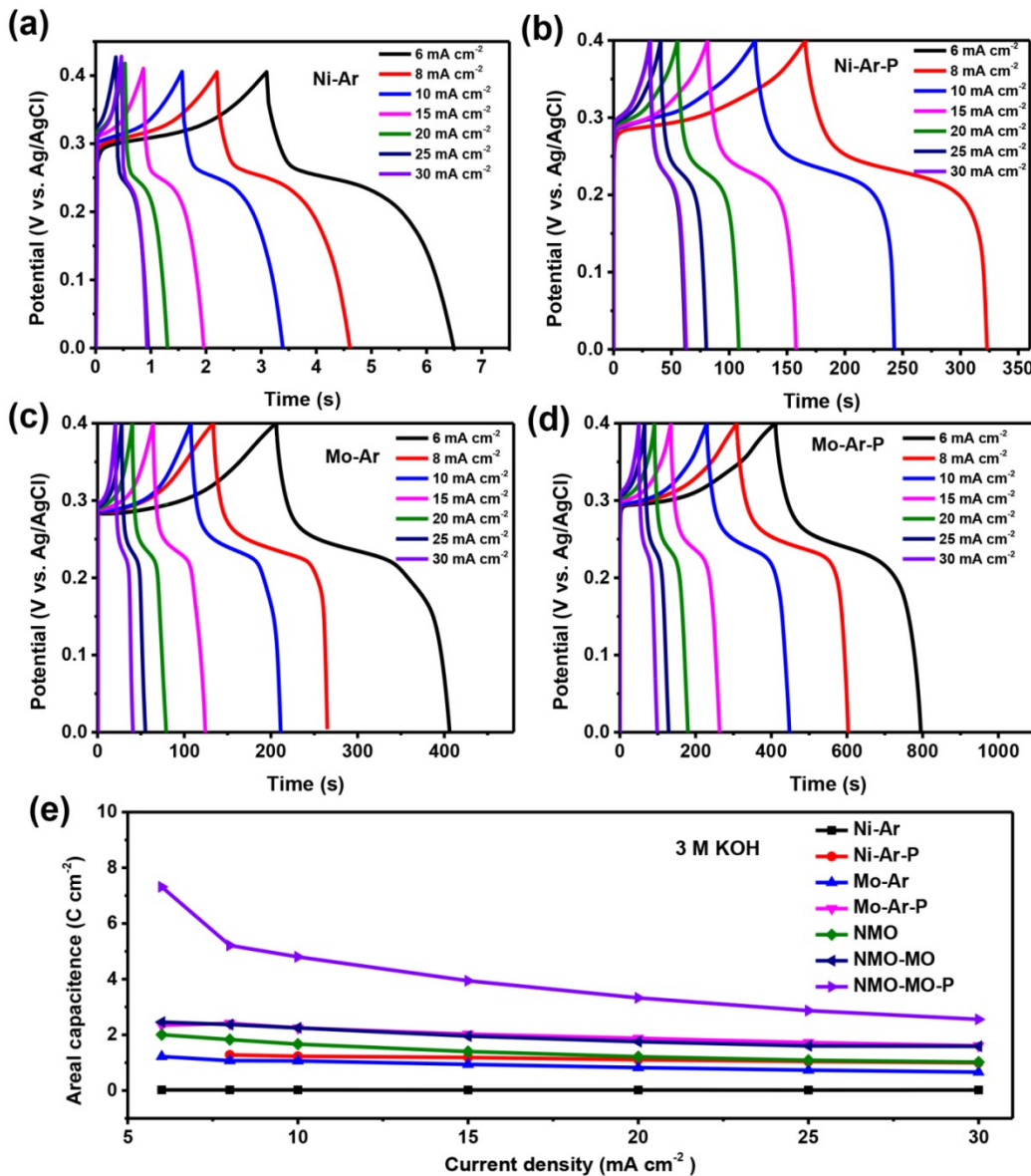


**Figure S15.** (a-d) GCD curves and (e) areal capacitance of the different electrodes as a function of current density in 3.0 M KOH.

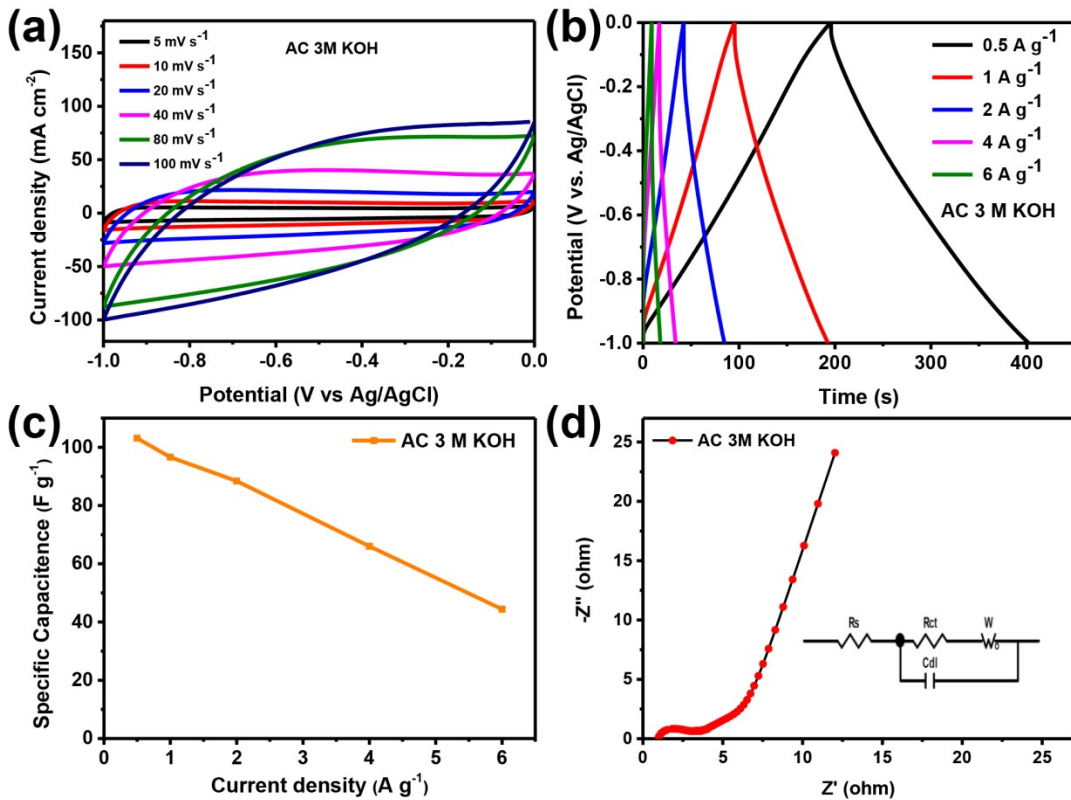


**Figure S16.** (a) CV curves, (b) GCD curves of AC electrode, (c) Specific capacitance and (d) Nyquist plots of the AC electrode.

**Table S3.** The parameters in the equivalent circuits of activated carbon (AC/NF).

Sample	$R_s$ ( $\Omega$ )	$R_{ct}$ ( $\Omega$ )	$W$ ( $\Omega$ )
Activated carbon on NF (AC/NF)	1.025	1.969	0.41

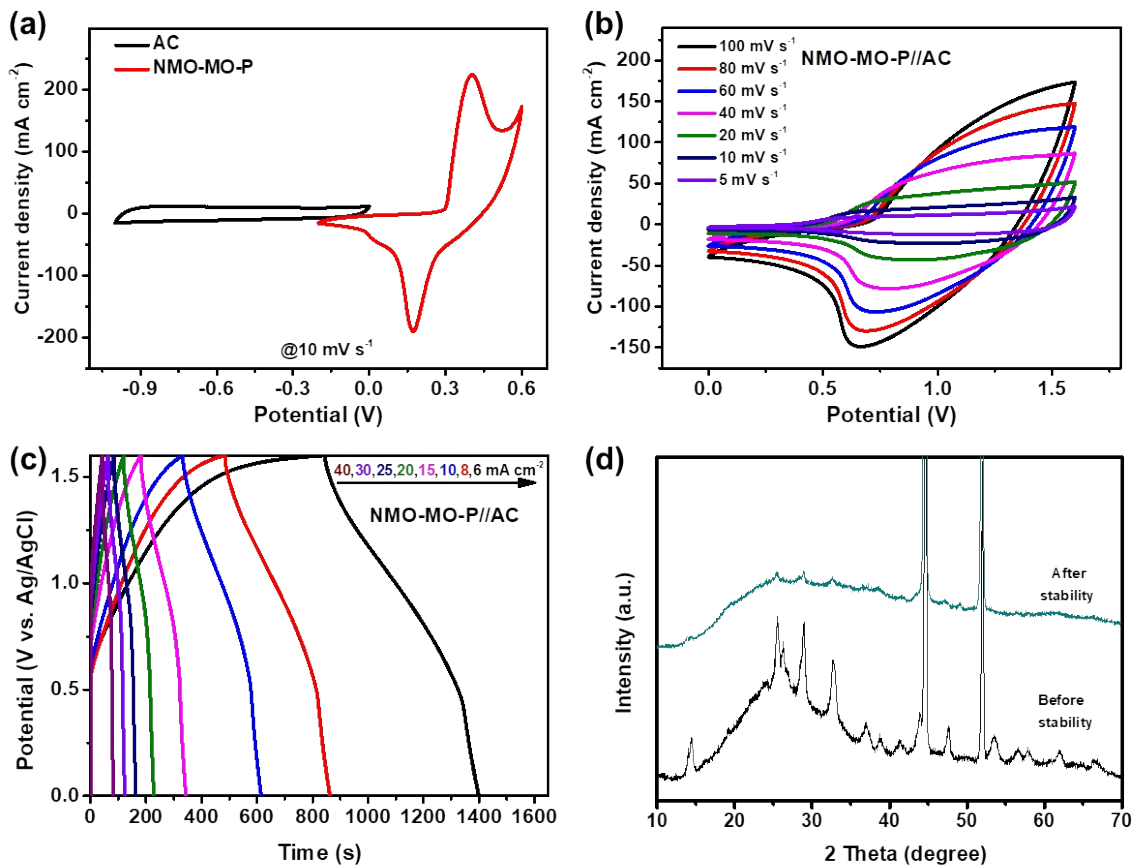


**Figure S17.** (a) CV curves of AC and NMO-MO-P electrodes at  $10 \text{ mV s}^{-1}$  in  $3.0 \text{ M KOH}$ . (b) CV curves at various scan rates and (c) GCD curves at different current densities of NMO-MO-P//AC device as a function of current density in  $3.0 \text{ M KOH}$ . (d) XRD spectra of NMO-MO-P before and after stability test.

**Table S4.** Comparison of the performances of the NMO-MO-P//AC with other NMO-based ASC.

ASC devices	Electrolyte	Operation voltage (V)	Energy density (Wh kg <sup>-1</sup> )	Power density (W kg <sup>-1</sup> )
NiMoO <sub>4</sub> /Ti <sub>3</sub> C <sub>2</sub> T <sub>x</sub> //rGH <sup>17</sup>	3 M KOH	1.6	33.36	400.08
NiCoMnO@NiMoO <sub>4</sub> @C//AC <sup>18</sup>	3 M KOH	1.6	59.9	214
CuO@NiMoO <sub>4</sub> //AC <sup>19</sup>	PVA/KOH	1.6	42.3	631.6
NiCo <sub>2</sub> O <sub>4</sub> @NiMoO <sub>4</sub> //AC <sup>20</sup>	6 M KOH	1.5	53.3	750
NiMoO <sub>4</sub> @NiS <sub>2</sub> /MoS <sub>2</sub> //Porous carbon <sup>21</sup>	6 M KOH	1.4	26.8	700
NiMoO <sub>4</sub> //AC <sup>22</sup>	6 M KOH	1.4	18	704
NiMoO <sub>4</sub> -CoMoO <sub>4</sub> //G-ink <sup>23</sup>	3 M KOH	1.5	27.58	636.05
Ag QDs/NiMoO <sub>4</sub> //AC <sup>24</sup>	3 M KOH	1.7	48.5	212.5
PCNS@Co <sub>0.21</sub> Ni <sub>0.79</sub> MoO <sub>4</sub> //AC <sup>25</sup>	2 M KOH	1.5	36.7	346.4
β-NiMoO <sub>4</sub> //rGO <sup>26</sup>	2 M KOH	1.5	29.3	187
<b>NMO-MO-P (Our work)</b>	<b>3 M KOH</b>	<b>1.6</b>	<b>55.36</b>	<b>359.4</b>
<b>NMO-MO-P (Our work)</b>	<b>2 M KOH</b>	<b>1.6</b>	<b>42.19</b>	<b>361.66</b>
<b>NMO-MO-P (Our work)</b>	<b>1 M KOH</b>	<b>1.6</b>	<b>24.29</b>	<b>364.24</b>

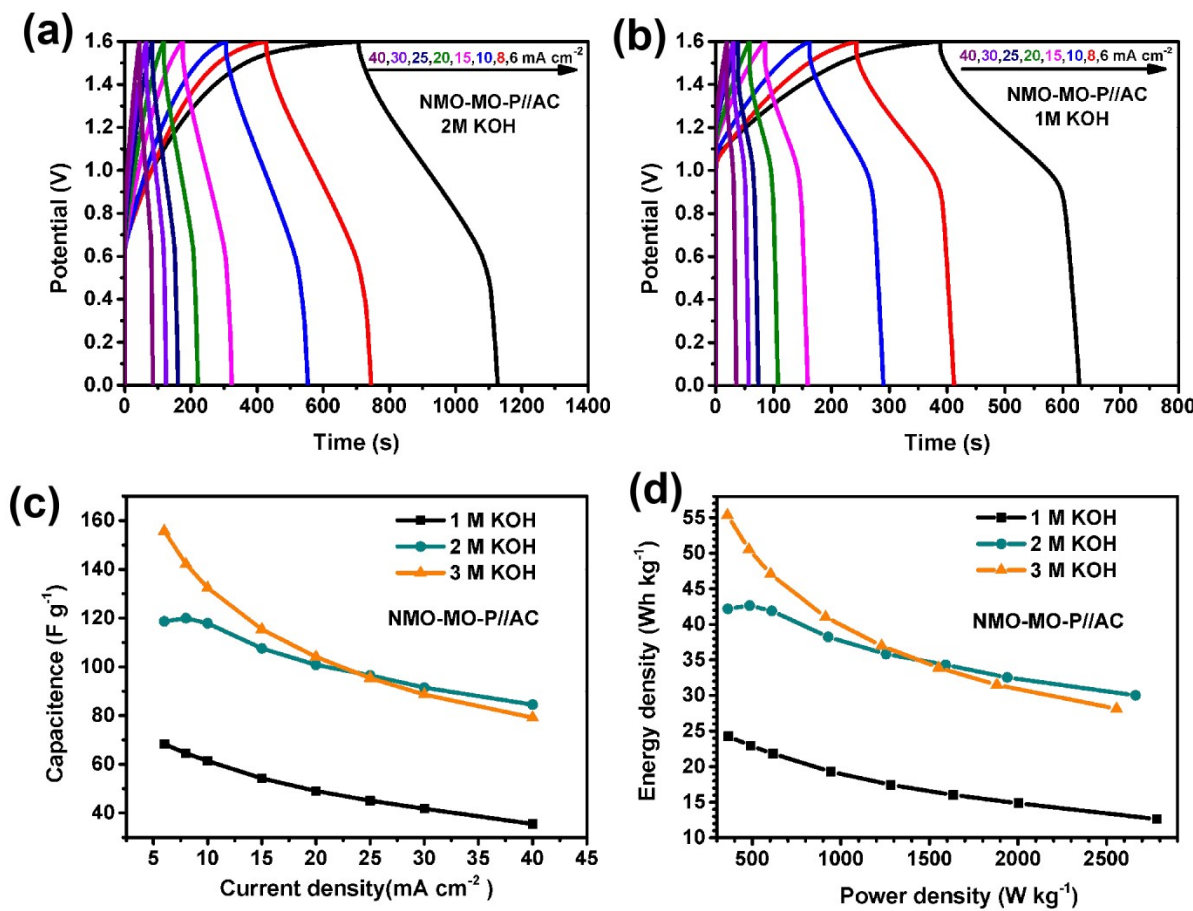


**Figure S18.** (a, b) GCD curves of NMO-MO-P//AC device at various current densities in 2.0 M KOH and 1.0 M KOH. (c) Specific capacitances as a function of current density and (d) Rate performance of NMO-MO-P//AC device in different concentrations of KOH.

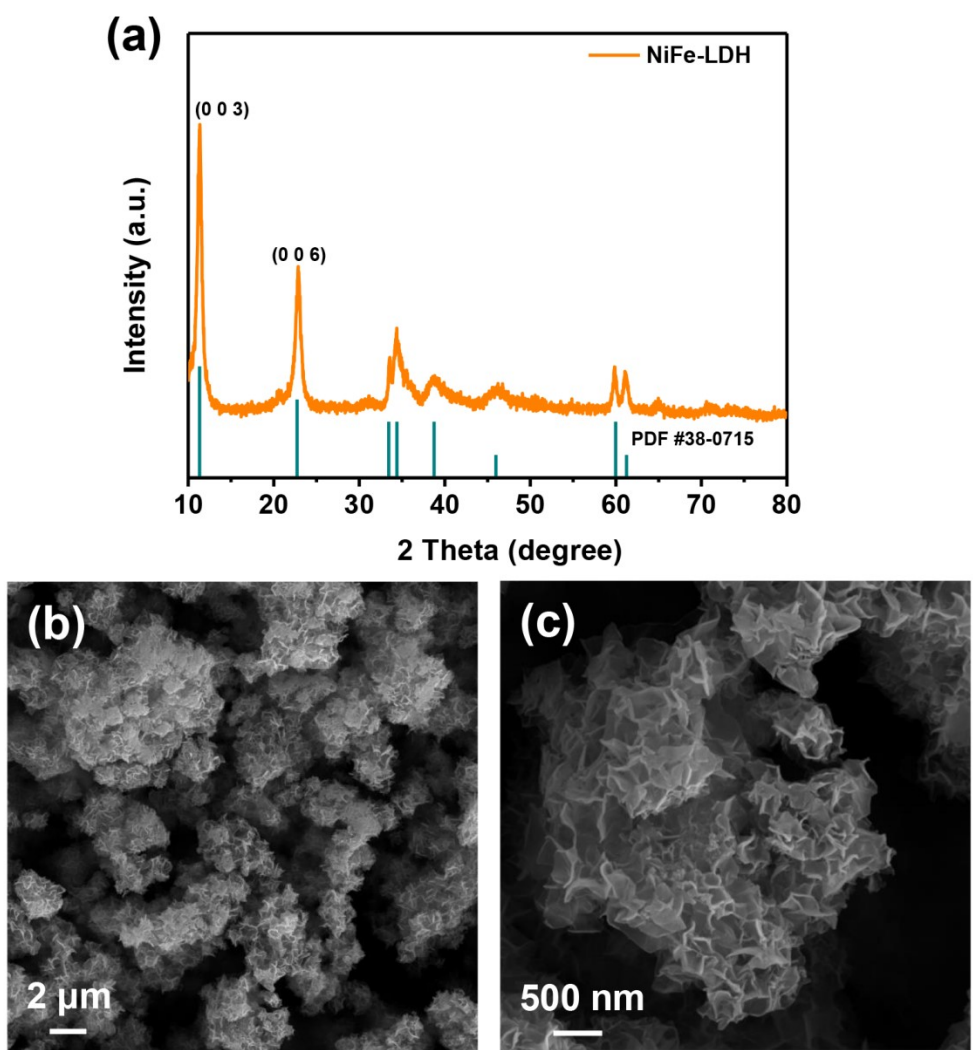


**Figure S19.** (a) XRD pattern, and (b-c) SEM images of NiFe-LDH.

**Table S5.** Comparison of the overall water splitting performance of our as-prepared NMO-MO-P NRs to other NMO-based catalysts in 1.0 M KOH electrolyte.

Electrocatalysts	OER (η@10 mA cm <sup>-2</sup> )	HER (η@10 mA cm <sup>-2</sup> )	OWS Voltage (V)
<b>NMO-MO-P (Our work)</b>	<b>241</b>	<b>23</b>	<b>1.50</b>
NiFe/NiMoO <sub>4</sub> /NiMoO <sub>4</sub> -P <sup>27</sup>	210	34	1.47
NiMoO <sub>4</sub> @MoSe <sub>2</sub> /Ni <sub>x</sub> Se <sub>y</sub> <sup>28</sup>	290	69	1.50
NF@P-Ni(OH) <sub>2</sub> /NiMoO <sub>4</sub> <sup>29</sup>	270	60	1.55
NiMoO <sub>4-x</sub> /MoO <sub>2</sub> <sup>30</sup>	233	41	1.56
NC/NiMo/NiMoO <sub>x</sub> <sup>31</sup>	284	29	1.57
NF@CoP <sub>3</sub> /NiMoO <sub>4</sub> <sup>32</sup>	347	92	1.57
CFC@N-NiMoO <sub>4</sub> /NiS <sub>2</sub> <sup>33</sup>	267	57	1.60
P-doped NiMoO <sub>4</sub> /NiMoO <sub>4</sub> ·nH <sub>2</sub> O <sup>34</sup>	260	148	1.62
NiCo <sub>2</sub> O <sub>4</sub> @NiMoO <sub>4</sub> <sup>35</sup>	300	170	1.65
NiMoO <sub>4</sub> //P-doped NiMoO <sub>4</sub> <sup>36</sup>	239	144	1.68

OWS: Overall water splitting

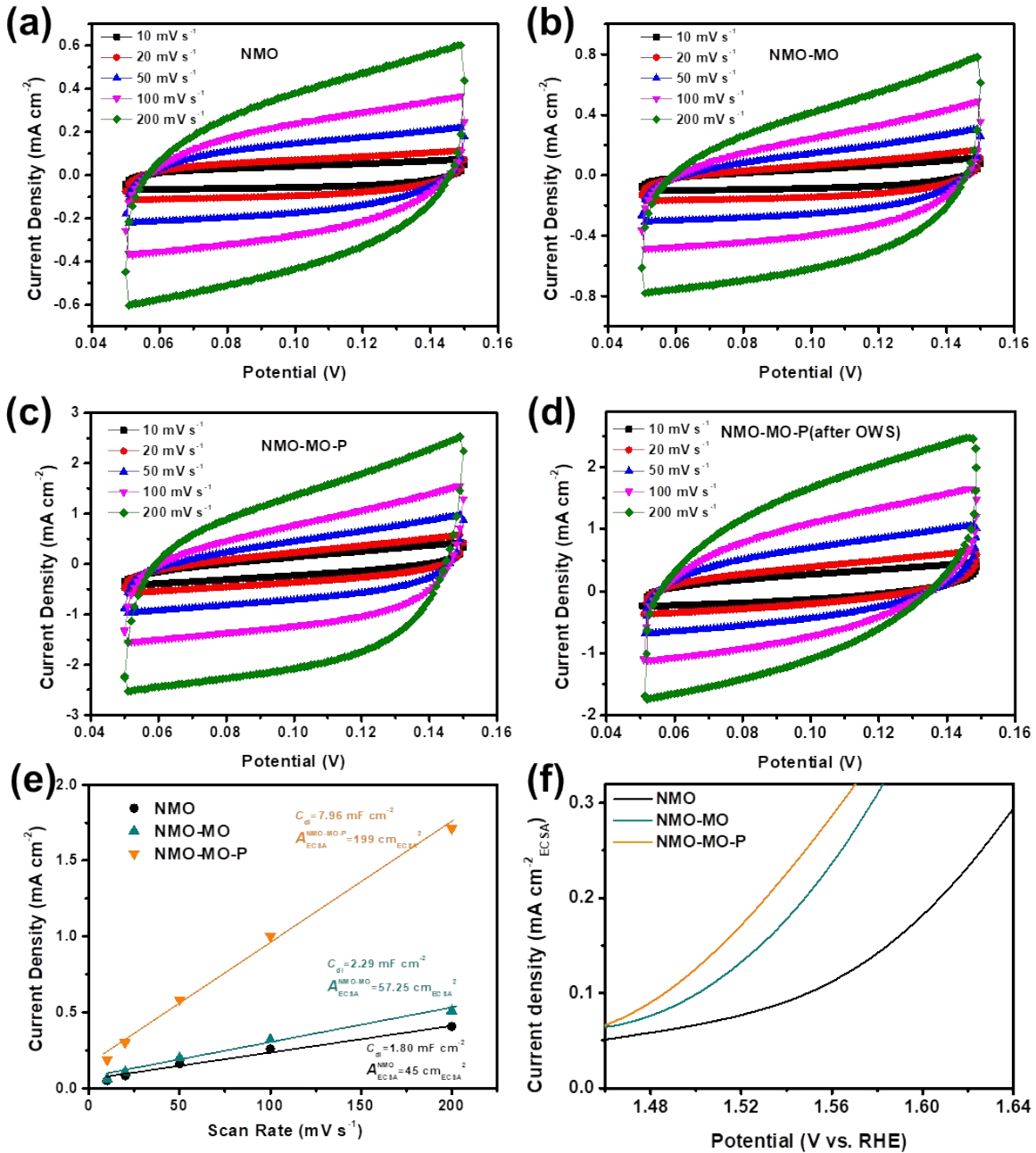


**Figure S20.** (a-c) CV curves (0.05 V ~ 0.15 V) at the different scan rates of the NMO, NMO-MO and NMO-MO-P catalysts. (d) CV curves (0.05 V ~ 0.15 V) at the different scan rates of the NMO-MO-P after OWS. (e) The corresponding ECSA values and (f) ESCA normalization.

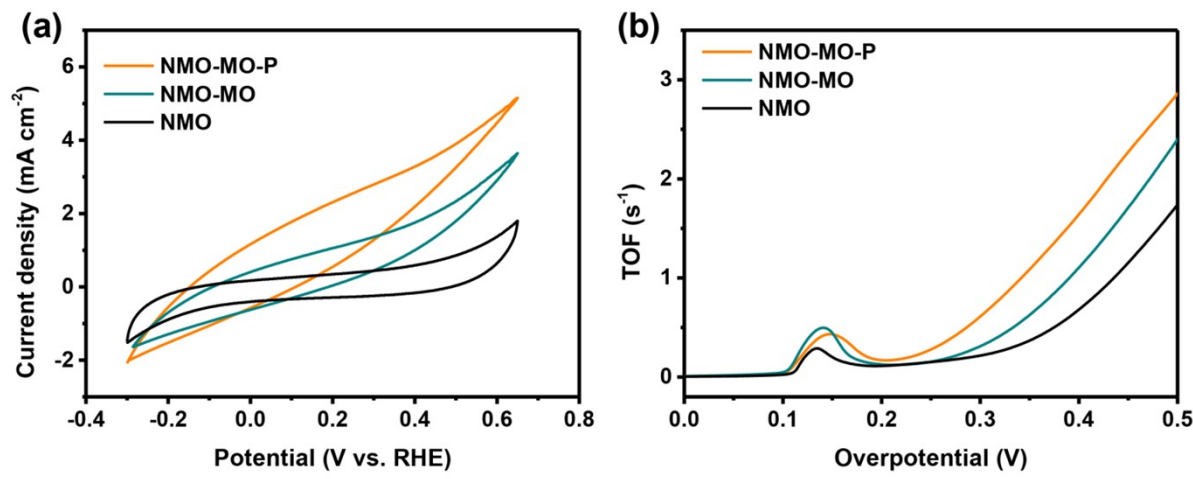


**Figure S21.** (a) CV curves of NMO, NMO-MO and NMO-MO-P in PBS solution (pH = 7.0) at a scan rate of  $50 \text{ mV s}^{-1}$ . (b) The TOFs of different catalysts.

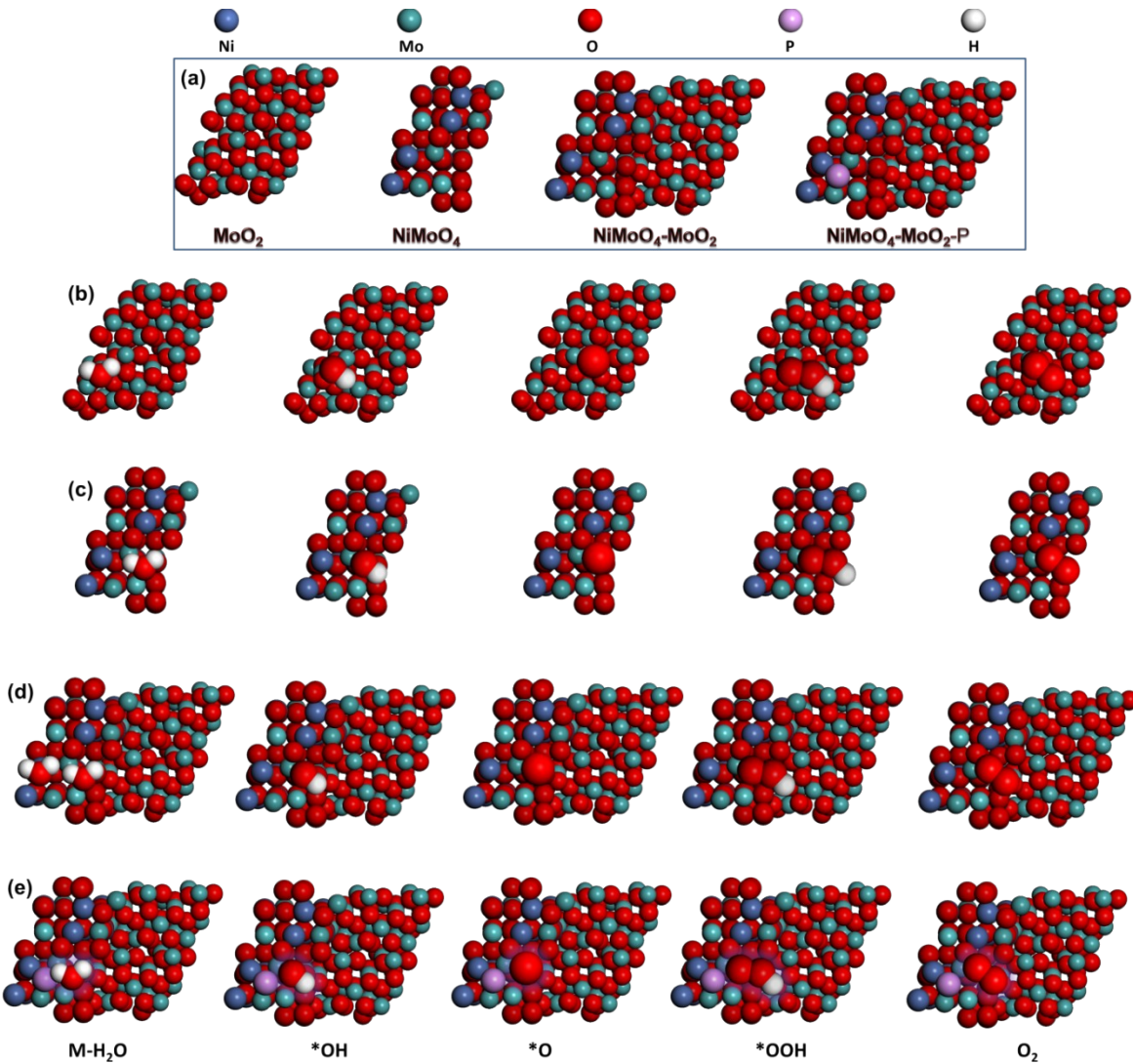


**Figure S22.** (a) Structural model of  $\text{MoO}_2$ ,  $\text{NiMoO}_4$ ,  $\text{NiMoO}_4\text{-MoO}_2$  and  $\text{NiMoO}_4\text{-MoO}_2\text{-P}$ . The model catalysts (b)  $\text{MoO}_2$ , (c)  $\text{NiMoO}_4$ , (d)  $\text{NiMoO}_4\text{-MoO}_2$  and (e)  $\text{NiMoO}_4\text{-MoO}_2\text{-P}$  with their corresponding intermediates adsorbed molecules.

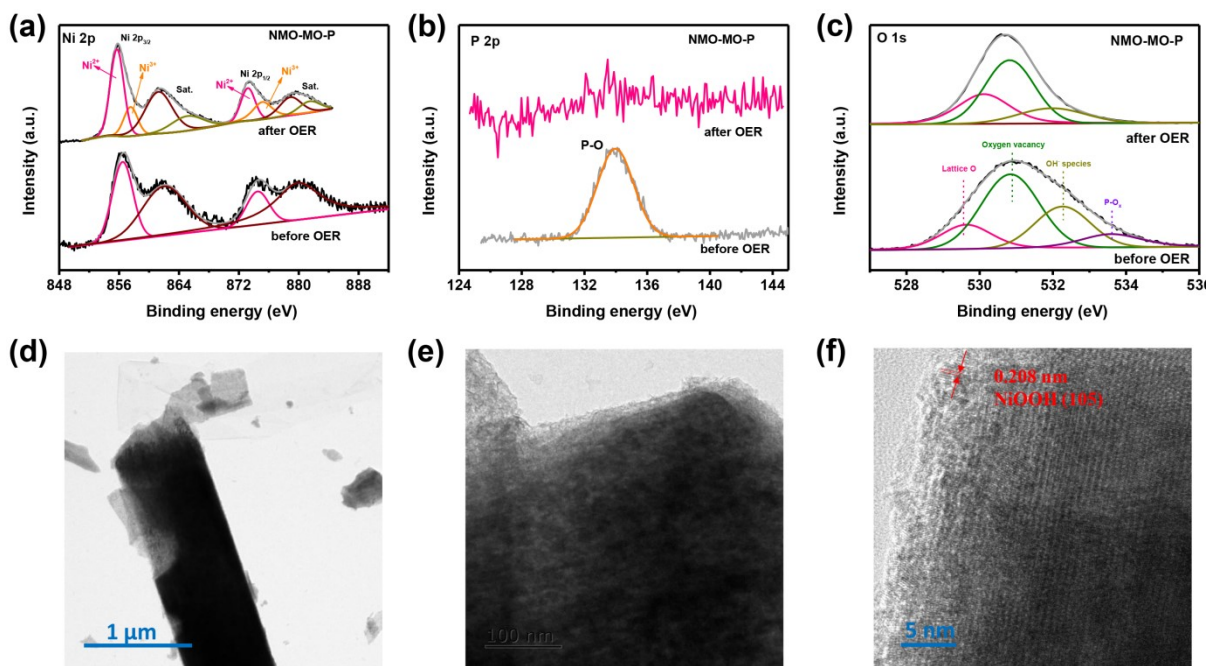


**Figure S23.** (a) Ni 2p, (b) P 2p and (c) O 1s XPS spectra of NMO-MO-P after OER stability test.

(d-f) TEM images of NMO-MO-P after OER stability test.

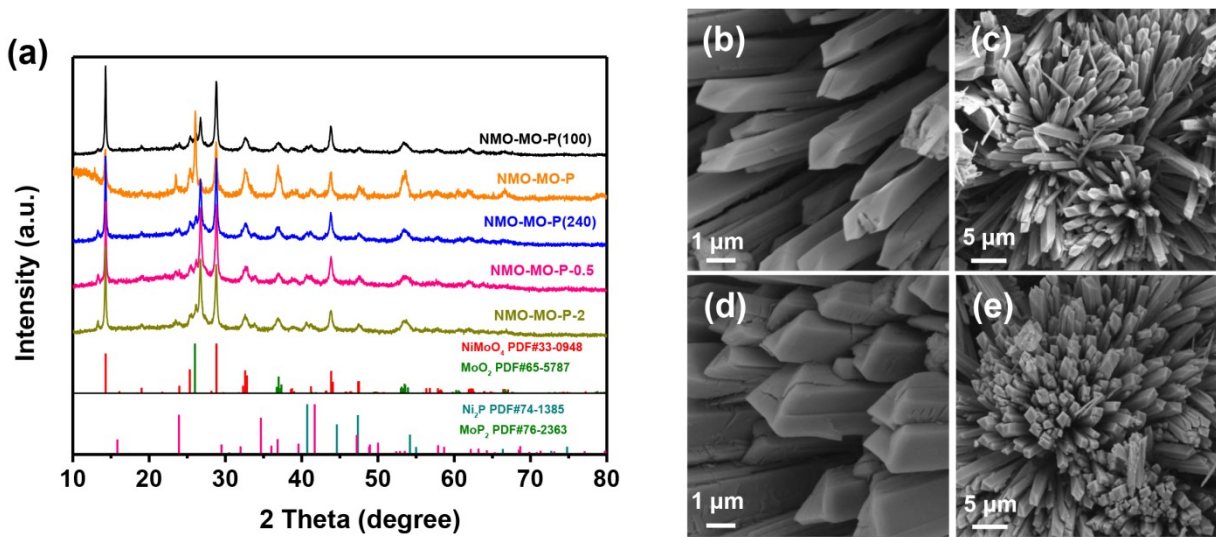


**Figure S24.** (a) XRD patterns. (b-e) SEM images of NMO-MO-P(100), NMO-MO-P(240), NMO-MO-P-0.5 and NMO-MO-P-2.

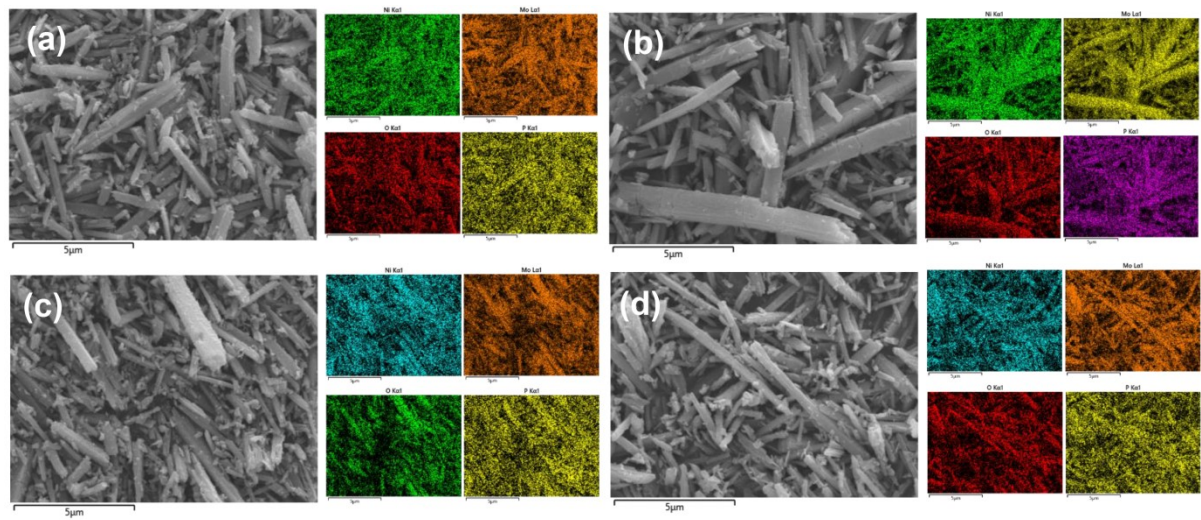


**Figure S25.** (a-d) SEM image and corresponding elements mapping of NMO-MO-P(100), NMO-MO-P(240), NMO-MO-P-0.5 and NMO-MO-P-2.

**Table S6.** Atom % of Ni, Mo, O and P in different samples analyzed using EDS.

Element Sample \	Ni	Mo	O	P
NMO-MO-P(100)	21.55	40.88	34.59	2.98
NMO-MO-P	19.37	43.68	31.99	4.96
NMO-MO-P(240)	20.54	40.03	32.89	6.54
NMO-MO-P-0.5	22.38	40.59	32.68	4.35
NMO-MO-P-2	20.56	42.09	32.06	5.29

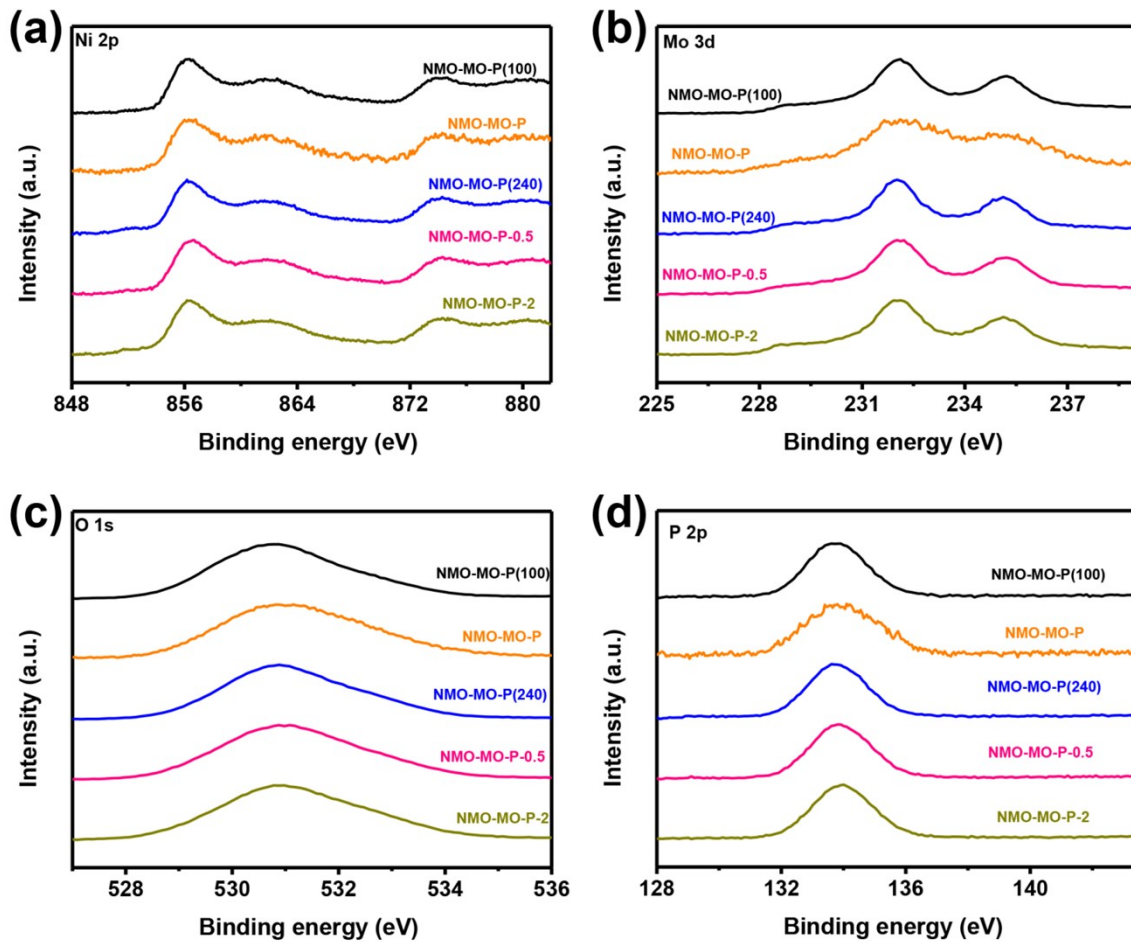


**Figure S26.** (a) Ni 2p, (b) Mo 3d, (c) O 1s and (d) P 2p XPS spectra of NMO-MO-P(100), NMO-MO-P(240), NMO-MO-P-0.5 and NMO-MO-P-2.

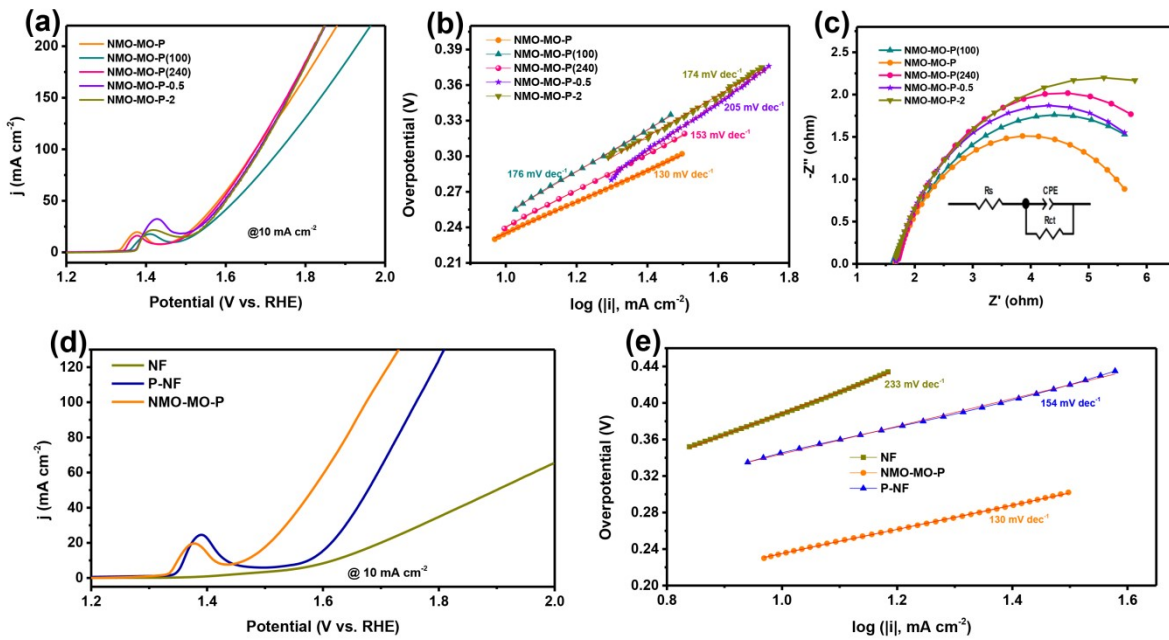


**Figure S27.** (a) LSV curves, (b) Tafel slopes and (c) Nyquist plots of NMO-MO-P(100), NMO-MO-P, NMO-MO-P(240), NMO-MO-P-0.5 and NMO-MO-P-2. (d) LSV curves and (e) Tafel slopes of NF, P-NF and NMO-MO-P.

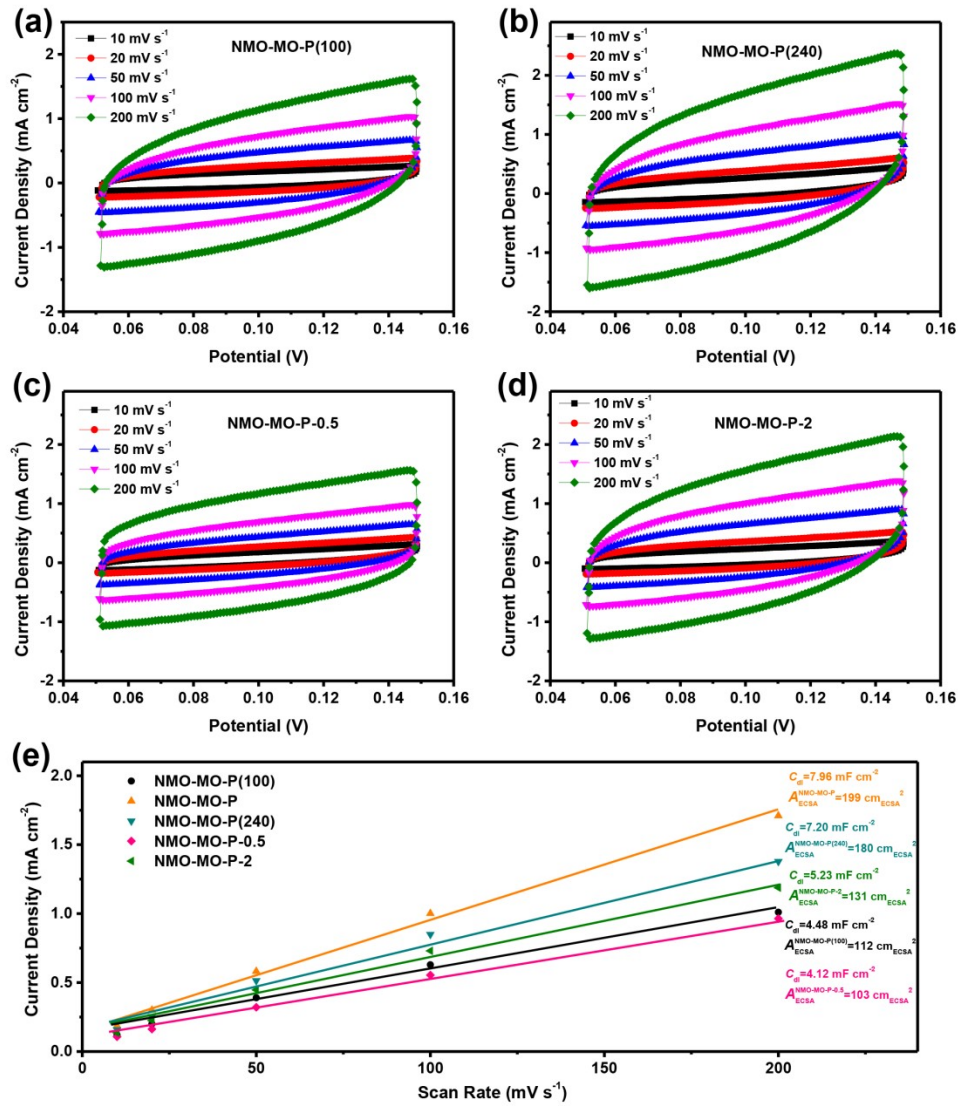


**Figure S28.** (a-c) CV curves ( $0.05 \text{ V} \sim 0.15 \text{ V}$ ) at the different scan rates of the NMO-MO-P(100), NMO-MO-P(240), NMO-MO-P-0.5 and NMO-MO-P-2. (e) The corresponding ECSA values.

**Table S7.** The parameters in the equivalent circuits of as-prepared electrocatalysts.

Electrocatalysts	$R_s$ (Ω)	$R_{ct}$ (Ω)
NMO-MO-P(100)	1.63	7.17
NMO-MO-P	1.66	5.14
NMO-MO-P(240)	1.71	7.69
NMO-MO-P-0.5	1.67	6.33
NMO-MO-P-2	1.68	9.57
Powder-NMO-MO-P	1.57	6.23

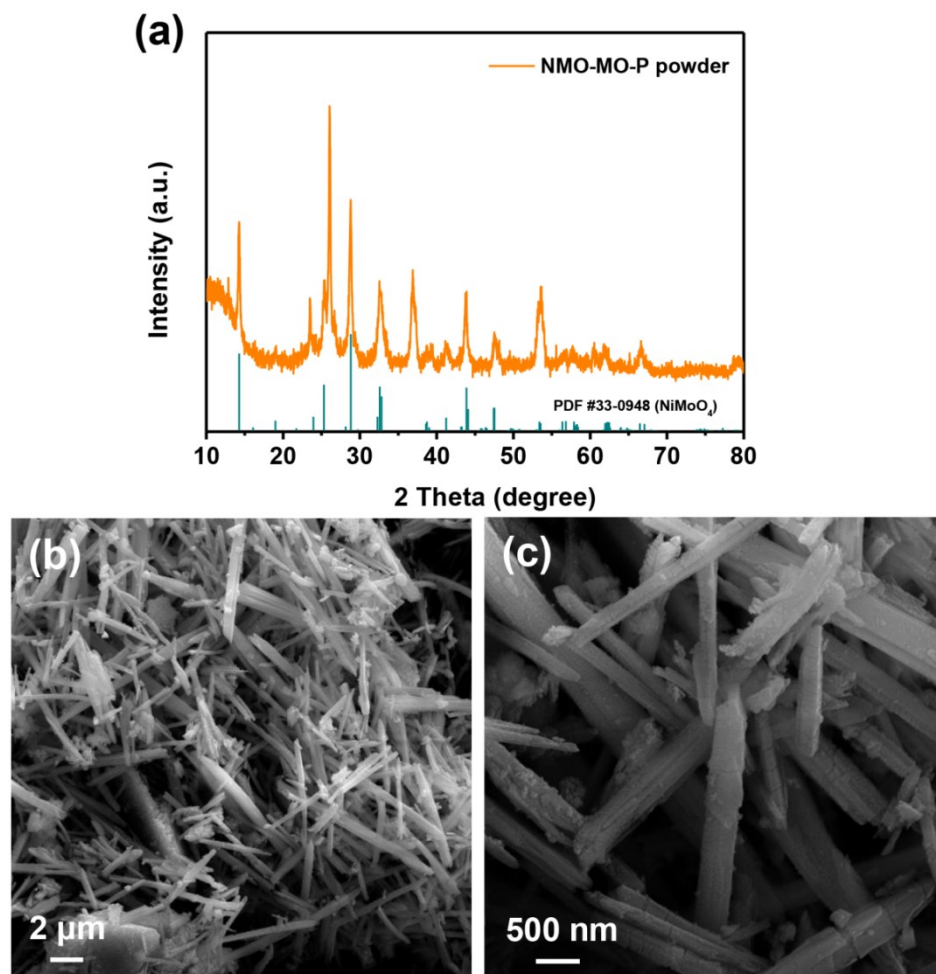


**Figure S29.** (a) XRD pattern of NMO-MO-P powder. (b-c) SEM images of NMO-MO-P powder.

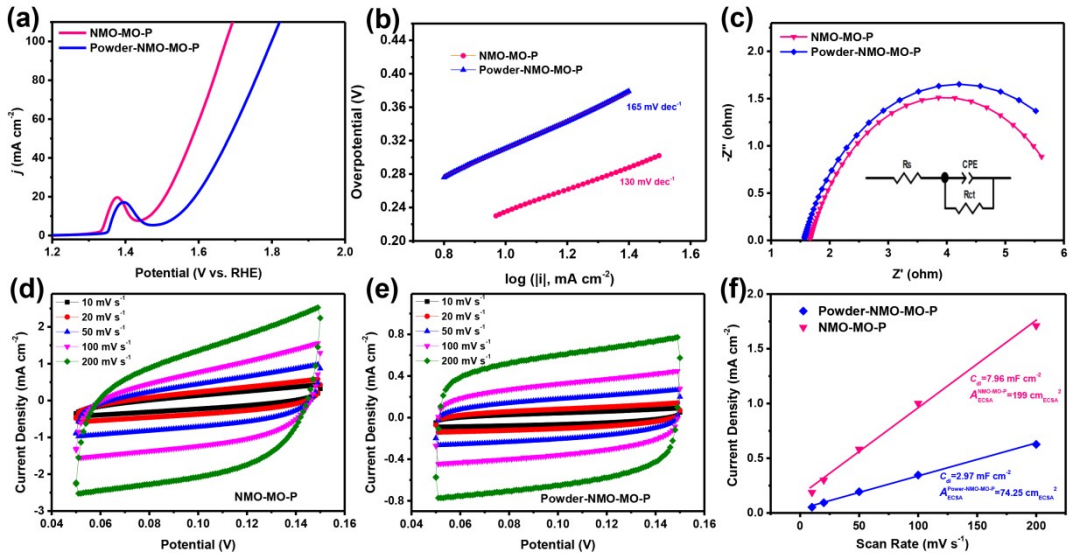


**Figure S30.** Alkaline OER electrochemical properties of the NMO-MO-P and powder-NMO-MO-P catalysts. (a) Polarization curves, (b) Tafel slope, (c) Nyquist plots, (d) ECSA values of NMO-MO-P and (e) powder-NMO-MO-P. (f) The corresponding ECSA values.

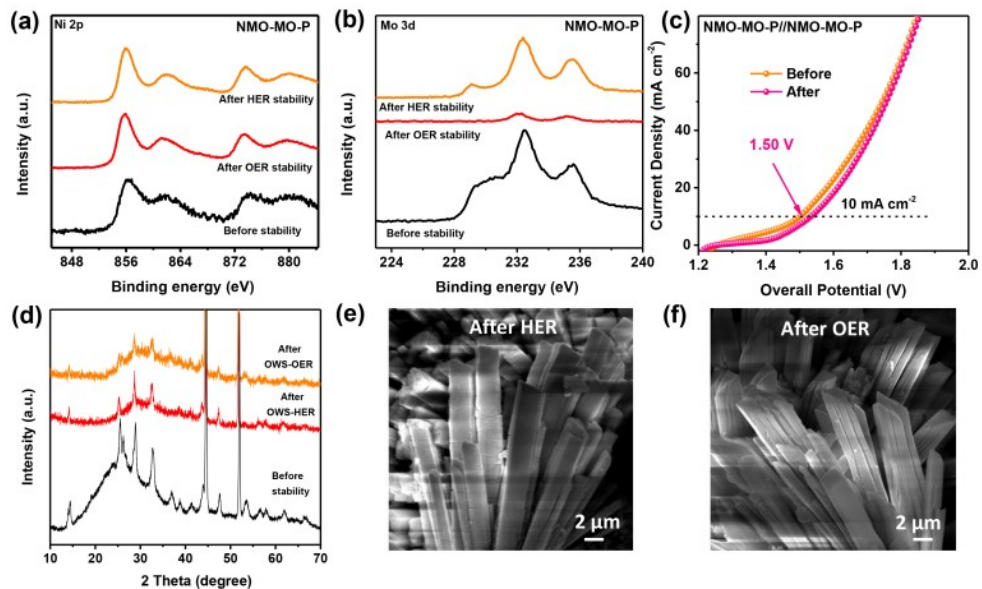


**Figure S31.** Post OWS analysis. (a) Ni 2p, (b) Mo 3d XPS spectra and (c) LSV curves of NMO-MO-P//NMO-MO-P device before and after stability test. (d) XRD spectra of NMO-MO-P before and after electrolysis. (e) HER and (f) OER SEM images of NMO-MO-P after OWS test.

After the OWS stability test, the strong electronic interaction in the NMO-MO-P catalyst was further confirmed by the unchanged electronic environments of both Ni 2p and Mo 3d XPS spectra compared to the untested NMO-MO-P sample (Figure S31a-b). The Mo severely dissolves more on the OER sample than the HER sample during the stability test, which can be identified by the Mo 3d XPS spectra peak intensities in Figure S31b and their corresponding Ni:Mo ratio of 1:0.04 for HER and 1:1.004 for OER compared to untested NMO-MO-P sample (Ni:Mo ratio of 1:2.18). However, the leaching did not cause any phase destruction, indicating of the NMO-MO-P crystal structure is preserved after the electrolytic test (Figure S31c).<sup>37, 38</sup> The device also maintained excellent stability after 12 h continuous electrolysis without significant degradation (Figure S31d). Furthermore, the dissolution of Mo did not cause any morphological destruction, indicating of the NMO-MO-P OER and HER samples morphology was preserved after the OWS test (Figure S31e-f). All these results further affirmed the excellent stability of the as-designed NMO-MO-P catalyst.

## References

1. X. Gonze, B. Amadon, P. M. Anglade, J. M. Beuken, F. Bottin, P. Boulanger, F. Bruneval, D. Caliste, R. Caracas, M. Côté, T. Deutsch, L. Genovese, P. Ghosez, M. Giantomassi, S. Goedecker, D. R. Hamann, P. Hermet, F. Jollet, G. Jomard, S. Leroux, M. Mancini, S. Mazevet, M. J. T. Oliveira, G. Onida, Y. Pouillon, T. Rangel, G. M. Rignanese, D. Sangalli, R. Shaltaf, M. Torrent, M. J. Verstraete, G. Zerah and J. W. Zwanziger, *Comput. Phys. Commun.*, 2009, **180**, 2582-2615.
2. J. P. Perdew and Y. Wang, *Phys. Rev. B*, 1992, **45**, 13244-13249.
3. M. J. van Setten, M. Giantomassi, E. Bousquet, M. J. Verstraete, D. R. Hamann, X. Gonze and G. M. Rignanese, *Comput. Phys. Commun.*, 2018, **226**, 39-54.
4. H. J. Monkhorst and J. D. Pack, *Phys. Rev. B*, 1976, **13**, 5188-5192.
5. W.-L. Ding, D.-M. Wang, Z.-Y. Geng, X.-L. Zhao and Y.-F. Yan, *J. Phys. Chem. C*, 2013, **117**, 17382-17398.
6. Y. Zhang, W.-d. Xue, H. Yin, D.-x. He and R. Zhao, *Composites Part A: Applied Science and Manufacturing*, 2018, **107**, 271-281.

7. J. Shen, Q. Wang, K. Zhang, S. Wang, L. Li, S. Dong, S. Zhao, J. Chen, R. Sun, Y. Wang, Z. Jian and W. Zhang, *Electrochim. Acta*, 2019, **320**, 134578.
8. L. Naderi and S. Shahrokhan, *J. Colloid Interf. Sci.*, 2019, **542**, 325-338.
9. P. Yao, C. Li, J. Yu, S. Zhang, M. Zhang, H. Liu, M. Ji, G. Cong, T. Zhang, C. Zhu and J. Xu, *J. Mater. Sci. Technol.*, 2021, **85**, 87-94.
10. S. Chen, S. Chandrasekaran, S. Cui, Z. Li, G. Deng and L. Deng, *Journal of Electroanalytical Chemistry*, 2019, **846**, 113153.
11. D. Zhu, X. Sun, J. Yu, Q. Liu, J. Liu, R. Chen, H. Zhang, D. Song, R. Li and J. Wang, *J. Colloid Interf. Sci.*, 2020, **574**, 355-363.
12. R. Xu, J. Lin, J. Wu, M. Huang, L. Fan, Z. Xu and Z. Song, *Appl. Surf. Sci.*, 2019, **463**, 721-731.
13. P. Zhang, J. Zhou, W. Chen, Y. Zhao, X. Mu, Z. Zhang, X. Pan and E. Xie, *Chem. Eng. J.*, 2017, **307**, 687-695.
14. Z. Zhu, W. Tian, X. Lv, F. Wang, Z. Hu, K. Ma, C. Wang, T. Yang and J. Ji, *J. Colloid Interf. Sci.*, 2021, **587**, 855-863.
15. Q. Shi, Q. Zhang, Y. Yang, Q. Zang, Z. Xiao, L. Zong, K.-P. Wang and L. Wang, *ACS Appl. Energy Mater.*, 2021, **4**, 801-809.
16. F. Wang, K. Ma, W. Tian, J. Dong, H. Han, H. Wang, K. Deng, H. Yue, Y. X. Zhang and W. Jiang, *J. Mater. Chem. A*, 2019, **7**, 19589-19596.
17. Y. Wang, J. Sun, X. Qian, Y. Zhang, L. Yu, R. Niu, H. Zhao and J. Zhu, *J. Power Sources*, 2019, **414**, 540-546.
18. X. Tang, Y. H. Lui, B. Zhang and S. Hu, *J. Power Sources*, 2020, **477**, 228977.
19. D. Yu, Z. Zhang, Y. Teng, Y. n. Meng, Y. Wu, X. Liu, Y. Hua, X. Zhao and X. Liu, *J. Power Sources*, 2019, **440**, 227164.
20. H. Zhang, C. Lu, H. Hou, Y. Ma and S. Yuan, *Chem. Eng. J.*, 2019, **370**, 400-408.
21. D. Chen, M. Lu, L. Li, D. Cai, J. Li, J. Cao and W. Han, *J. Mater. Chem. A*, 2019, **7**, 21759-21765.
22. N. S. Neeraj, B. Mordinia, A. K. Srivastava, K. Mukhopadhyay and N. E. Prasad, *Appl. Surf. Sci.*, 2019, **473**, 807-819.

23. C. V. V. M. Gopi, S. Sambasivam, K. V. G. Raghavendra, R. Vinodh, I. M. Obaidat and H.-J. Kim, *Journal of Energy Storage*, 2020, **30**, 101550.
24. X. Zhang, Z. Li, Z. Yu, L. Wei and X. Guo, *Appl. Surf. Sci.*, 2020, **505**, 144513.
25. J. Lin, L. Yao, Z. Li, P. Zhang, W. Zhong, Q. Yuan and L. Deng, *Nanoscale*, 2019, **11**, 3281-3291.
26. X. Lu, W. Jia, H. Chai, J. Hu, S. Wang and Y. Cao, *J. Colloid Interf. Sci.*, 2019, **534**, 322-331.
27. S. Zhuang, S. Tong, H. Wang, H. Xiong, Y. Gong, Y. Tang, J. Liu, Y. Chen and P. Wan, *Int. J. Hydrot. Energy*, 2019, **44**, 24546-24558.
28. Z. Zhang, S. Ye, J. Ji, Z. Li and F. Wang, *Colloids and Surfaces A: Physicochemical and Engineering Aspects*, 2020, 124888.
29. W. Xi, G. Yan, H. Tan, L. Xiao, S. Cheng, S. U. Khan, Y. Wang and Y. Li, *Dalton Transactions*, 2018, **47**, 8787-8793.
30. Z. Zhang, X. Ma and J. Tang, *J. Mater. Chem. A*, 2018, **6**, 12361-12369.
31. J. Hou, Y. Wu, S. Cao, Y. Sun and L. Sun, *Small*, 2017, **13**, 1702018.
32. Y.-Q. Wang, L. Zhao, X.-L. Sui, D.-M. Gu and Z.-B. Wang, *Ceram. Int.*, 2019, **45**, 17128-17136.
33. L. An, J. Feng, Y. Zhang, R. Wang, H. Liu, G.-C. Wang, F. Cheng and P. Xi, *Adv. Funct. Mater.*, 2019, **29**, 1805298.
34. R. Jiang, D. Zhao, H. Fan, Y. Xie, M. Li, H. Lin and Z.-S. Wu, *J. Colloid Interf. Sci.*, 2022, **606**, 384-392.
35. D. Cui, R. Zhao, J. Dai, J. Xiang and F. Wu, *Dalton Transactions*, 2020, **49**, 9668-9679.
36. Y. Song, W. Sha, M. Song, P. Liu, J. Tian, H. Wei, X. Hao, B. Xu, J. Guo and J. Liang, *Ceram. Int.*, 2021, **47**, 19098-19105.
37. G. Solomon, A. Landström, R. Mazzaro, M. Jugovac, P. Moras, E. Cattaruzza, V. Morandi, I. Concina and A. Vomiero, *Adv. Energy Mater.*, 2021, **11**, 2101324.
38. W. Du, Y. Shi, W. Zhou, Y. Yu and B. Zhang, *Angew. Chem. Int. Ed.*, 2021, **60**, 7051-7055.